Phase separation in lipid-based nanoparticles: exploring the nano-bio interface

Papadopoulou, P.

CHAPTER 4

Structure-function relationship of phase-separated liposomes containing diacylglycerol analogues

Panagiota Papadopoulou[#], Gabriela Arias-Alpizar[#], Pim Weeda, Thijs Poppe, Niels van Klaveren, Tomas Slíva, Dennis Aschmann, Winant van Os, Yun Zhang, Mohammad-Amin Moradi, Nico Sommerdijk, Frederick Campbell, Alexander Kros*

# denotes equal contribution
ready for submission

Abstract | Composition and morphology of lipid-based nanoparticles can influence their overall *in vivo* behavior. Previously, we demonstrated that phase separation in liposomes composed of DSPC and a diacylglycerol lipid analogue (DOaG), drives the *in vivo* biodistribution towards a specific subset of endothelial cells in zebrafish embryos. In the absence of traditional targeting functionalities (*e.g.*, antibodies, ligands), this selectivity is mediated solely by the unique liposome morphology, characterized by a DOaG-rich lipid droplet within the DSPC-rich phospholipid bilayer. The phase separationis induced due to the geometry of DOaG lipid and its ability to create non-bilayer phases in lipid membranes. To investigate the underlying principles of phase separation and to optimize the liposome colloidal stability, we performed a structure-function relationship study by synthesizing a library of DOaG analogues varying molecular properties, such as the number, length and *sn*-position of the acyl chains, as well as the degree of saturation or carbonyl substituents. We assessed the ability of these lipid analogues to assemble into phase-separated liposomes and studied their morphology, colloidal stability, and *in vivo* biodistribution in zebrafish embryos. We found that analogues containing unsaturated, medium length (C16-C18) fatty acids were required to obtain colloidally stable, phase-separated liposomes with cell-specific biodistribution patterns. Moreover, we observed that using the pure DOaG isomer, with acyl chains at the *sn*-1,3 positions leads to more colloidally stable liposomes than when a mixture of *sn*-1,2 and *sn*-1,3 isomers is used. Similarly, we observed that incorporating a DOaG analogue with fatty tails shorter than DSPC, as well as PEGylation, favor liposome long term stability while retaining cell-selective biodistribution. Diacylglycerols are known to promote fusion, lipid polymorphism, signaling and protein recruitment on lipid membranes. In this study we showed that diacylglycerol derivatives can induce phase separation in liposomes, unlocking the potential for cell-specific targeting *in vivo*. We believe these findings can be the foundation for future use of diacylglycerols in lipid-based nanomedicines and could lead to the development of novel targeted delivery strategies.

4.1 Introduction

Composition and molecular properties of lipids used in lipid-based nanoparticles play a pivotal role on their overall *in vivo* behavior. Charge, geometry and degree of saturation, as well as combination of different lipids and molar ratios, dictate lipid nanoparticle size, morphology, rigidity and surface chemistry. Upon *in vivo* administration, these physicochemical properties influence the protein corona formation, clearance, cell uptake and endocytic routes, thereby controlling the overall nanoparticle biodistribution.[1–4] However, the underlying principles are still only understood at a basic level, limiting the effective design of nanomedicines with a high therapeutic efficacy.

Whereas strong surface charge – either anionic or cationic – appears to lead to dominant interactions in the body, [5–10] the fate of neutral lipid nanoparticles appears more nuanced.[1,3,9,10] Geometry of individual lipids contributes to lipid polymorphism[11,12] and controls the morphological and physicochemical properties of lipid-based nanoparticles, which in turn determine the particle - protein interactions and *in vivo* fate. [13–16] Inverted conical lipids with bulky polar head groups result in assemblies with positive curvature (*i.e.*, micelles), while lipids with cylindrical geometry result in planar lamellar bilayers (*i.e.*, liposomes).[11,17] Conical lipids with small polar headgroups increase the negative curvature of membranes providing fusogenic properties in lipid-based nanoparticles[11,18] and facilitate endosomal escape after endocytosis, a crucial event for drug and nucleic acid delivery.[15,19,20] Additionally, conical lipids can lead to non-bilayer phases *i.e.*, inverse hexagonal phase (H_{II}).[17,21–24] One example of such lipids are diacylglycerols (DAGs).[25] DAGs are endogenous lipids found in the cell membrane – mainly after the hydrolysis of phosphatidylinositol – and activate enzymes such Protein Kinase C (PKC) or Phospholipase C, promoting signaling cascade.[25] Lacking a phosphate group, DAGs are hydrophobic conical lipids which can occupy the interleaflet space of lamellar lipid membranes. Above a critical concentration in the bilayer, local accumulation of DAGs disrupts the lamellar properties of membranes, and leads to phase separation and formation of lipid droplets buried within the phospholipid leaflet.[26–30]

In a recent study, we demonstrated how DAG-induced phase separation can drive the biodistribution of liposomes to specific endothelial cell types in zebrafish embryos.[13] The liposome formulation (denoted PAP3) consisting of an equimolar mixture of the saturated, naturally occurring, phospholipid DSPC (1,2-distearyl-*sn*-glycero-3-phosphatidylcholine, T*m* = 55 ºC) and a synthetic DAG analogue, DOaG (2-hydroxy-3-oleamidopropyl-oleate, or dioleoylamidoglycerol), resulted in phase-separated liposomes bearing a single lipid droplet in each bilayer (**Figure 1a, b**). Surprisingly, upon intravenous administration in zebrafish embryos, PAP3 liposomes selectively accumulated within brain endothelial cells (bECs) without the use of traditional targeting ligands (*e.g.*, antibodies, peptides) (**Figure 1c**). The observed liposome recognition and accumulation in bECs was mediated by triglyceride lipase (TGL), which is highly present at the luminal surface of zebrafish bECs during development. Importantly, we showed that this process required the presence of the phase-separated droplet within the liposome bilayer, implying a preferential nanoparticle-protein communication due to unique morphology and composition.[13,14] Additionally, we found that accumulation of DOaG within the DSPC leaflet induced lipid packing defects on the liposome surface, exposing the DOaG to the surrounding environment, a key factor for the specific interaction between PAP3 liposomes and TGL.[14] As with DAGs, DOaG increases the distance between adjacent phospholipids, increasing hydrophobicity and facilitating recognition and binding of TGL on the lipid membrane.[14,29,31]

In this study, we designed a library of close DOaG analogues, to probe how the exact molecular chemistry and structure of DOaG induce phase separation in liposomes and concomitant bEC targeting in embryonic zebrafish. Chain length, degree of saturation, number and *sn*-position of fatty acid chains, and carbonyl substituents on the backbone, were varied to study the effect on lipid assembly and *in vivo* cell-specific targeting (**Figure 1d**). Hence, molecular DOaG analogues were synthesized, mixed with DSPC (analogue/DSPC 1:1) and assembled into liposomes. Long-term stability and morphology of the resulting liposomes were characterized by dynamic light scattering (DLS) and cryo-transmission electron microscopy (cryo-TEM) respectively, and their *in vivo* behavior was assessed in zebrafish embryos (**Figure 1e**).

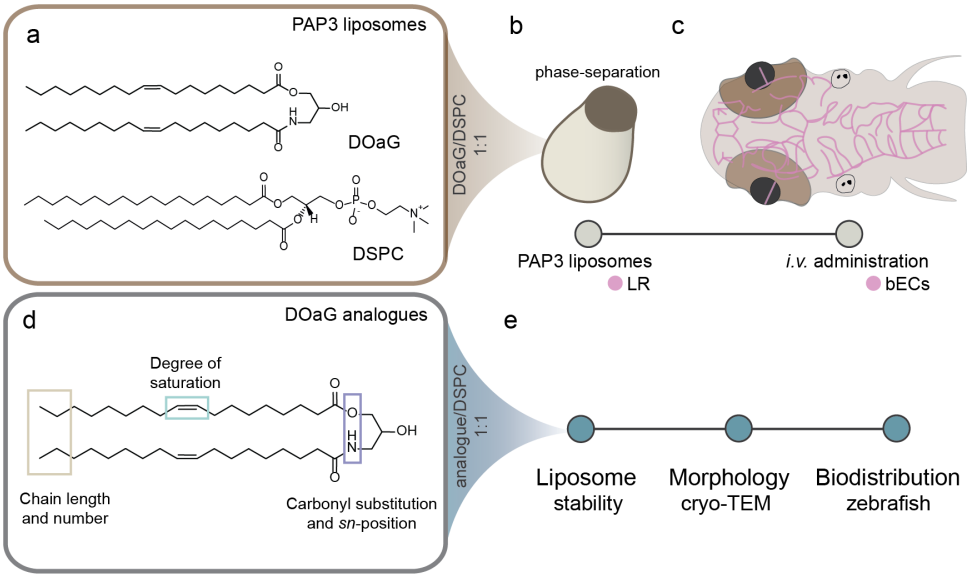

Figure 1. Overview of phase-separated liposomes and timeline of experiments. a) Molecular structures of DOaG and DSPC. **b)** Schematic of phase-separated liposomes containing DOaG and DSPC (1:1). **c)** Schematic dorsal view of zebrafish embryo head. Injected liposomes contained 0.2% mol DOPE-LR (1,2-dioleoyl-sn-glycero-3-phosphoethanolamine-N-[lissamine rhodamine B sulfonyl]) for visualization. (Brain) vasculature depicted in pink, region in which liposomes selectively accumulate. **d)** Molecular properties of DOaG which were altered to generate a library of DOaG analogues. **e)** Overview of DOaG library assessment: Liposomes were formulated from a 1:1 ratio of DSPC:analogue and stability, morphology and biodistribution were assessed by DLS, cryo-TEM and confocal imaging of injected zebrafish embryos, respectively.

Overall, we observed that DOaG analogues with unsaturated, medium length (C16-C18) fatty acid tails – when co-formulated with DSPC – can induce phase separation in colloidally stable liposome formulations, which leads to bEC specific biodistribution patterns in embryonic zebrafish. Monoacyl and triacyl glycerol analogues, as well as diacyl analogues with saturation, or shorter (C14) or longer fatty acid tails (C20-C24), either i) cannot form liposomes, or ii) phase separationexists only in a small fraction of the population, or iii) the formulation cannot interact with bECs. Additionally, we show the naturally occurring dioleoylglycerol (DOG) retains the properties of DOaG, proving the correlation of

the well-studied DAGs in membranes with the DOaG-induced phase-separation. Finally, we show that lipids with fatty acid tails substituting the *sn*-1,3 positions of the backbone result in liposomes with more favorable long-term stability, than when the *sn*-1,2 positional isomer is also present in the formulation. Similarly, PAP3 liposomes could be stabilized by a small amount of DMPE-PEG2k (1,2-dimyristoyl-sn-glycero-3-phosphoethanolamine-N-[methoxy(polyethylene glycol)-2000), or by replacing DOaG with the shorter (C16:1) analogue. This improved the long-term stability and ability to assemble liposomes in physiologically relevant buffers, which is particularly important for the translation towards nanomedicine formulations with high therapeutic efficacy.

4.2 Results and Discussion

Molecular library of DOaG analogues

DOaG is a synthetic, amide-containing analogue of dioleoylglycerol (DOG) (**Figure 2a, b**). It is mainly isolated as a mixture of two positional isomers – something that also occurs in natural lipids – in which the two acyl chains substitute the *sn*-1,3 positions and *sn*-1,2 positions with a 8:2 ratio **(Figure S1**). To understand the influence of individual molecular properties of the DOaG lipid, a library of 12 analogues was created, maintaining the glycerol-like backbone in all newly synthesized lipids (**Figure 2b**). Firstly, a series of changes in chain length was generated, altering the monounsaturated fatty acid chains, from C14:1 to C24:1, resulting in lipids **1-5** (**Figure 2c** and **Figure S2b, g**. Note: lipid 3 is DOaG). Subsequently, degree of saturation was altered (**Figure 2d** and **Figure S2c, g**), with either full saturation on both C18 tails (lipid **6**) one saturated and one monounsaturated tail (lipid **7**) or with di-unsaturation in both tails (lipid **8**). Next, we generated lipids with only one, or three oleic chains and lipids with either two esters (naturally occurring DAG), or two amides (**Figure 2e, f** and **Figure S2d-e, g, lipids 9-12**). Finally, to assess the importance of the regioisomeric mixture of positional isomers, we synthesized the pure DOaG isomer with substitution on the *sn*-1,3 position (~ 95% pure), as a comparison of the mixture that has been studied so far (*sn*-1,3/80%, *sn*-1,2/20%) (lipid **21, Figure 2g** and **Figure S2f, g**).

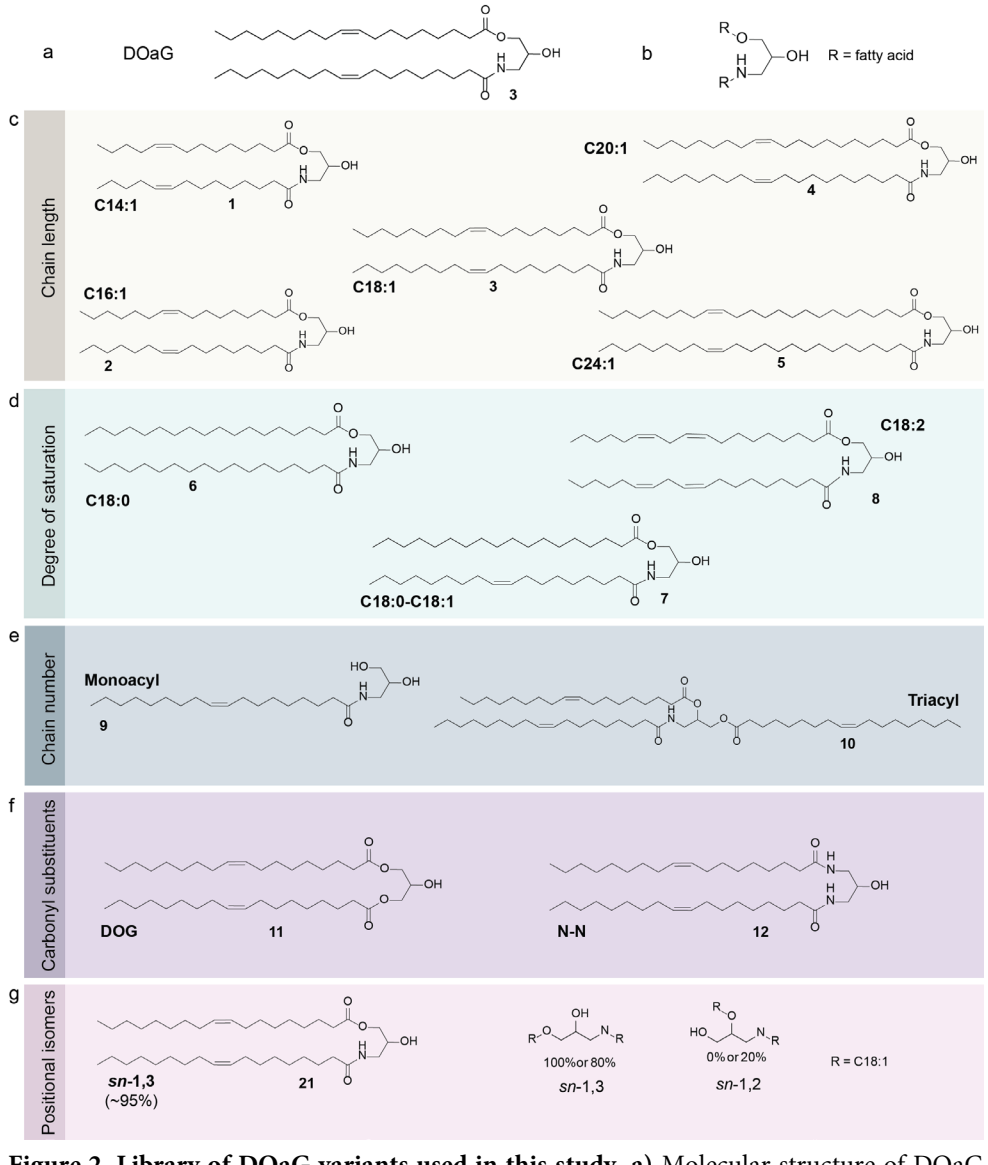

Figure 2. Library of DOaG variants used in this study. a) Molecular structure of DOaG lipid. **b)** DOaG glycerol-like backbone. DOaG analogues varying the: **c)** chain length, **d)** degree of saturation, **e)** number of acyl chains, **f)** carbonyl substituents of the glycerol-like backbone and **g)** *sn*-position of acyl chain substitution. All lipids exist as a regioisomeric mixture of *sn*-1,3 and *sn*-1,2 positional isomers (8:2 ratio), except for (**7**, **9**, **10**, **12**, **21**). Only the *sn*-1,3 isomer is shown for clarity.

Chain length influences stability and bEC targeting

Liposomes containing an equimolar mixture of DSPC and the **C14:1** analogue (**lipid 1**), were stable over a period of ~25 days, maintaining their hydrodynamic diameter below 200 nm albeit with the polydispersity increasing after 6 days (**Figure 3a**). The majority (80%) of the liposomes revealed a phase-separated morphology (**Figure 3b**) as quantified by cryo-TEM (**Figure S3a, d**). Interestingly, real-time biodistribution imaging in zebrafish suggested these liposomes mostly accumulate in a subset of cells located in the tail region of the zebrafish embryo, named as scavenging endothelial cells[6] and in the zebrafish liver, but not in bECs despite their phase-separated morphology (**Figure 3c** and **Figure S4a, b**). We hypothesize the **C14:1** analogue might be too short to create high packing defects at the liposome membrane, resulting in less exposure to the surrounding environment therefore being less recognizable by TGL. Liposomes assembled from the **C16:1** analogue (**lipid 2**) were stable over a period of 30 days and monodisperse (**Figure 3d**). Phase separation was also observed in these liposomes, while the bilayers appeared less cornered (less flat) suggesting a more liquid disordered phase than the **C14:1** containing liposomes (**Figure 3e, Figure S3b**). This indicates that **C16:1** analogues are able to mix with the DSPC-rich membranes more effectively due to a smaller chain length mismatch. Therefore, the membrane becomes more flexible resulting in more spherical liposomes with less corners. Quantification indicated that the large majority of liposomes (~90%) possessed a phase-separated morphology (**Figure S3d**). Liposomes containing the **C16:1** variant were also able to target bECs (**Figure 3f** and **Figure S4c, d)**, similar to the original PAP3 liposomes[13] which contain **C18:1** chains (DOaG, **lipid 3** in figure 2c) (compare **Figure 3f** with **Figure 3i** and **Figure S4e, f)**. Extending the unsaturated chain length by 2 carbons (**C18:1**) decreased the stability of the resulting liposomes, as these were only stable and monodisperse for less than 7 days (**Figure 3g**). The membrane of the phase-separated **C18:1** containing liposomes appeared more fluid as evidenced by the more spherical shape of the liposomes compared to the **C14:1** and **C16:1** variants (**Figure 3h** and **Figure S3c**). Similar to **C16:1** containing liposomes, **C18:1** containing liposomes were predominantly phase-separated (**Figure S3d**). Further extension of the acyl chains to **C20:1** DOaG analogue (**lipid 4**), resulted in

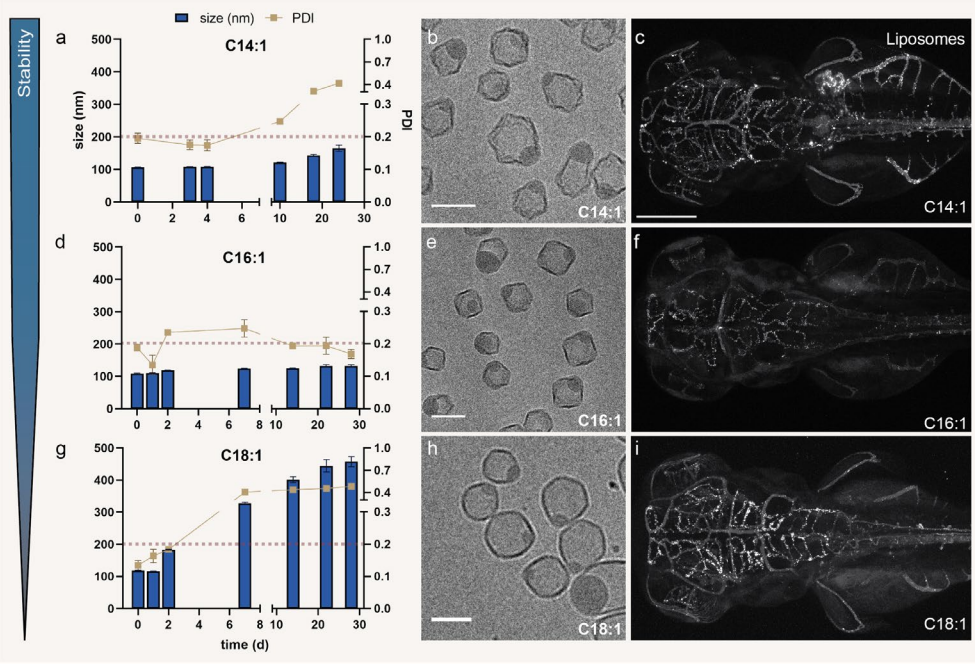

Figure 3. Stability, morphology and biodistribution of liposomes consisting of DSPC and DOaG analogues (1:1) as a function of chain length. Size (nm) and polydispersity index (PDI) of liposomes consisting of DSPC and **a)** C14:1, **d)** C16:1, **g)** C18:1 variant over a period of ~30 days. Cryo-TEM image of liposomes consisting of DSPC and **b)** C14:1, **e)** C16:1, **h)** C18:1 variant. Biodistribution of liposomes (grey) consisting of DSPC and **c)** C14:1, **f)** C16:1, **i)** C18:1 variant in a Tg(*kdrl*:GPF) zebrafish embryo, in dorsal view (10x magnification), 1.5 hour post injection (hpi) at 78 days post fertilization (dpf). Liposomes consisting of 1:1 DSPC/analogue, total lipid concentration 5 mM containing 0.2 mol% DOPE-LR (dioleoyl-phosphatidylethanolamine-lissamine rhodamine). Scale bars: 200 µm for zebrafish and 100 nm for cryo-TEM images. Dynamic light scattering (DLS) was used to obtain data in a, d and g. Size as determined by the measurement of the hydrodynamic diameter (nm). Red dashed line in a, d and g indicates the threshold of size and PDI relevant for *in vivo* use. Cryo-TEM imaging at d=0.

aggregation after only ~6 h (**Figure S5a**), while the **C24:1** variant (**lipid 5**) did not assemble into liposomes at all (**Figure S5b**).

These findings, as well as the instability of the **C18:1**-containing formulation (PAP3), indicate that liposomes progressively aggregate by increasing fatty acid chain length, when mixed with DSPC.

This supports previous findings which show DOaG is exposed to the surrounding environment due to large hydrophobic packing defects induced in the membrane, due to phase-separation.[14] Hence, the longer the fatty acid tail of the variant the more the variant is exposed to the surroundings and therefore the shorter the stability of the overall assembly and vice versa. We have reported previously that packing defects on PAP3 liposomes are a key factor for liposome recognition by TGLs,[14] which in turn influences liposome uptake *in vivo*.[13] Liposomes which contain the shorter chain (**C14:1**) analogue did not target bECs but *are* phase-separated. A possible explanation for this observation is that packing defects on these liposomal membranes are lower throughout.

C14:1 lipids may possibly be more buried within the leaflet and less exposed on the liposome surface, due to their shorter chains and high mismatch with DSPC, therefore the liposome surface is less favorable for protein recruitment. Increasing the chain length by two carbons (**C16:1** analogue) is already enough to create liposomes that target bECs, indicating again the starting point of exposure and accessibility of the lipid. This in turn, indicates **C16:1** creates fewer packing defects than the longer **C18:1** (DOaG) lipid and so forth. This hypothesis is supported by the colloidal stability studies, in which **C16:1** containing liposomes are shown to be more stable and less prone to aggregation, than the **C18:1** containing liposomes. Since liposomes with > C18 chains do not form stable formulations, **C16:1** and **C18:1** lipid seem to be the "sweet spot" for phase-separation, liposome stability and bEC targeting.

Unsaturated analogues favor liposome formation and phase separation

We next assessed the effect that unsaturation in DOaG analogues has on the liposome assembly, by synthesizing a fully saturated variant (**C18:0, lipid 6**). This analogue could not be formulated into liposomes with DSPC as a co-formulant (**Figure S6a**). The intermediate lipid analogue **C18:0-C18:1 (lipid 7)** was also unable to assemble into stable liposomes (**Figure S6b**). This confirmed that both acyl chains must be unsaturated in order to assemble into stable phase-separated liposomes with DSPC. Indeed, as with DOaG, similar results were obtained with the DOaG analogue with two (conjugated) double bonds in each fatty acid tail (**C18:2, lipid 8**). Liposomes made of DSPC/C18:2 (1:1) were stable for at least 30 days, albeit

with a moderate PDI (**Figure 4a**). Cryo-TEM analysis showed these liposomes were predominantly phase-separated (**Figure 4b** and **Figure S7a, e**), but the bilayers appeared to be more in the gel-phase, as evidenced by cornered/flat membranes. The double unsaturation per acyl chain has a strong influence on the lipid's geometry and we assume the packing on this lipid within the DSPC leaflet might be more compact and completely de-mixed from DSPC, resulting in a gel-phase for the bilayer. Liposomes containing **C18:2** were able to target bECs in zebrafish embryos (**Figure 4c and Figure S9a, b**). In conclusion, equimolar mixtures of unsaturated DOaG analogues and DSPC assemble into phase separated liposomes, which in turn are able to selectively target bECs *in vivo*.

Influence of chain number and amide in glycerol-like backbone

Next, we investigated how essential the number of acyl chains per glycerol is for phase-separation. Monoacylglycerols have been studied before for their ability to form inverse hexagonal and (inverse) cubic liquid crystalline phases.[23,24] However, a liposome formulation with (1:1) DSPC and a **monoacyl** variant (**lipid 9**), formed liposomes that were highly unstable, as evidenced by the rapid size increase within ~6 h (**Figure S6d**). The **triacyl** variant (**lipid 10**), formulated with DSPC, formed liposomes that were stable for at least 30 days (**Figure 4d**). Interestingly, these liposomes were predominantly lamellar in morphology (~80%), with some solid particles (~2%) and only a small fraction (~5%) which revealed a phase-separated morphology (**Figure 4e** and **Figure S7b, e**). As a result, the majority of injected liposomes in zebrafish did not accumulate in the brain endothelium (**Figure 4f and Figure S9c, d**). Only a minor fraction was able to target bECs, which might be explained by the fraction of phase-separated liposomes in the formulation. To assess the influence of the ester and amide functionalities of DOaG on phase separation and *in vivo* bEC targeting, we synthesized the naturally occurring dioleoylglycerol (**DOG, lipid 11**). Liposomes containing **DOG** were stable in size and with acceptable PDI values for a period of 20 days (**Figure 4g**). Similar to **PAP3** liposomes, the **DOG** containing-liposomes revealed a phase-separated morphology (**Figure 4h** and **Figure S7c),** albeit for only ~55% of all liposomes (**Figure S7e**). DOG/DSPC liposomes also targeted bECs (**Figure 4i**). Interestingly, the lipid analogue with two amides (coded **N-N, lipid 12**) could not be formulated into stable liposomes (**Figure S6c**). A possible explanation may be an additional hydrogen bond due to the introduction of the extra amide, thereby negatively influencing lipid assembly into defined nanoparticles.

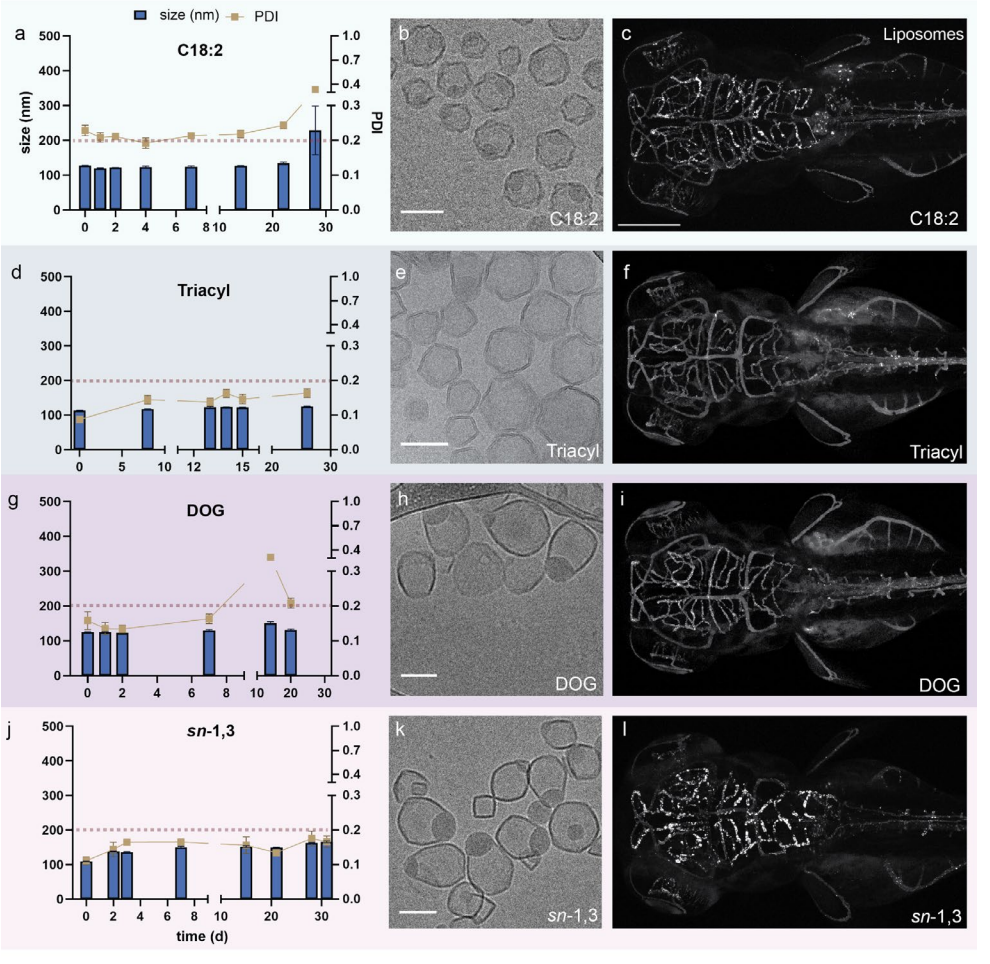

Figure 4. Stability, morphology and *in vivo* behavior of liposomes consisting of DSPC and DOaG analogues (1:1) as a function of saturation, number of fatty acid tails, carbonyl substitution or *sn*-position substitution. Size (nm) and PDI of liposomes consisting of DSPC and **a)** C18:2, **d)** Triacyl, **g)** DOG, **j)** *sn*-1,3 variant over a period of ~30 days. Cryo-TEM image of liposomes consisting of DSPC and **b)** C18:2, **e)** Triacyl, **h)** DOG, **k)** *sn*-1,3 variant. Biodistribution of liposomes (grey) consisting of DSPC and **c)** C18:2, **f)** Triacyl, **i)** DOG, **l)** *sn*-1,3 variant in a Tg(kdrl:GPF) zebrafish embryo, in dorsal view (10x magnification), 1.5 hpi at 78 dpf. Liposomes consisting of 1:1 DSPC/analogue, total lipid concentration 5 mM containing 0.2 mol% DOPE-LR. Scale bars: 200 µm for zebrafish and 100 nm for cryo-TEM images. DLS was used to obtain data in a, d, g and j. Size as determined by the measurement of the hydrodynamic diameter (nm). Red dashed line in a, d, g and j indicates the threshold of size and PDI relevant for *in vivo* use. Cryo-TEM imaging at d=0.

***Sn*-position in fatty acid tails influences stability**

Due to the chosen synthetic strategy, all previously discussed DOaG lipids (except lipid 7, 9, 10 and 12) were a mixture of the *sn*-1,2 and *sn*-1,3 isomers with a ~2:8 ratio. Therefore, we synthesized the *sn*-1,3 isomer in high purity (~95%, coded ***sn*-1,3, lipid 21**) and upon co-assembly with DSPC, stable liposomes were obtained for at least 30 days (**Figure 4j**). In contrast, the original PAP3 liposomes, that contained the *sn*-1,3/*sn*-1,2 mixture, were only stable for 7 days (**Figure 3g**). As expected, liposomes with *sn*-1,3 were phase-separated (**Figure 4k** and **Figure S7d**), with only a small population (3.3%) having an unknown, highly structured liquid-crystalline phase (**Figure S7d, e** and **Figure S8**), with a repeat distance of 4.85 nm as seen by Fast Fourier Transform (FFT) analysis. Biodistribution studies in zebrafish embryos revealed that liposomes containing this isomerically pure DOaG variant were also able to target bECs in a selective manner (**Figure 4l** and **Figure S9g, h**).

C16:1 variant and PEGylation improves long term stability

Despite their interesting morphology and selective *in vivo* behavior, PAP3 liposomes are not stable in physiologically isosmotic and isotonic buffers which contain saline (*i.e.*, phosphate buffered saline [PBS]). This is particularly important for the efficient applicability of these liposomal formulations towards nanomedicine. PAP3 liposomes formulated in water are stable for 7 days, however in PBS rapid aggregation is observed (**Figure 5a, b**). This is likely due to the lack of ability of membranes which contain DAGs to coordinate sodium ions, as described in a previous study;[32] and although formulating liposomes containing the pure ***sn*-1,3** DOaG variant (*i.e.*, excluding the *sn*-1,2 isomer) improves the overall stability of PAP3 liposomes, it does not improve their stability in PBS (**Figure S10**). Interestingly, when co-formulated with DSPC, the shorter (**C16:1**) lipid variant could formulate stable phase-separated liposomes in PBS, with colloidal stability for at least 30 days and with improved PDI values (**Figure 5a, d**). This supports our hypothesis that **C16:1** lipids are less exposed to the aqueous surroundings than DOaG, leading to less membrane instability and aggregation. Alternatively, a low percentage of PEGylated lipid also increased the stability of PAP3 liposomes, while retaining morphology and bEC targeting. Previously, addition of 5% mol of DSPE-PEG2k-(1,2-distearoyl-sn-glycero-3-phosphoethanolamine-N-amino(polyethylene

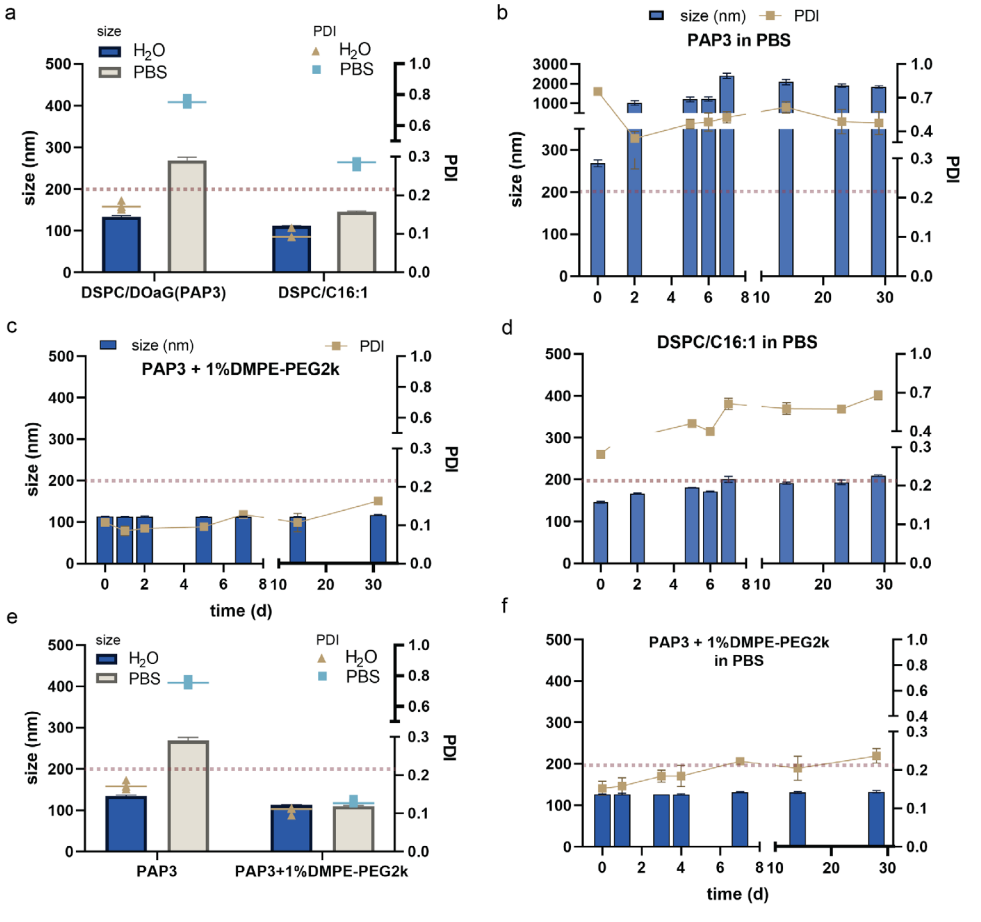

Figure 5. Optimization and stability studies of PAP3 liposomes. a) Size (nm) and PDI of PAP3 liposomes (DSPC/DOaG) or DSPC/C16:1 liposomes, formulated in ddH_2O or PBS. **b)** Size (nm) and PDI of PAP3 liposomes formulated in PBS over a period of ~30 days. **c)** Size (nm) and PDI of PAP3 liposomes incorporating 1 % mol DMPE-PEG2k formulated in ddH_2O over a period of ~30 days. **d)** Size (nm) and PDI of DSPC/C16:1 liposomes formulated in PBS over a period of ~30 days. **e)** Size (nm) and PDI of PAP3 liposomes or PAP3 liposomes incorporating 1 % mol DMPE-PEG2k, formulated in ddH_2O or PBS. **f)** Size (nm) and PDI of PAP3 liposomes incorporating 1 % mol DMPE-PEG2k formulated in PBS over a period of ~30 days. DLS was used to obtain the data depicted in this figure. Size as determined by the measurement of the hydrodynamic diameter (nm). Red dashed line indicates the threshold of size and PDI relevant for *in vivo* use.

glycol)-2000) in PAP3 was observed to abolish the bEC targeting.[13] Addition of only 1% mol of DMPE-PEG2k however, showed to be optimal, keeping the *in vivo* bEC targeting while also improving liposomal stability (**Figure 5c**). PAP3 liposomes with 1% mol DMPE-PEG are phase-separated (**Figure S11)** and target bECs in zebrafish embryos (**Figure S12).** Importantly, when formulated in PBS, stability of PAP3 liposomes incorporating 1% mol of DMPE-PEG2k was improved even further than the **C16:1** variant (**Figure 5e, f**). The information obtained by this effort to optimize the phase-separated liposomes can be the basis for future developments, or use of DAGs and DAG analogues in lipid-based formulations.

Saturation in phospholipid co-formulant is important for phase separation

It is important to mention that liposomes with DOaG and the fluid DOPC (1,2-dioleoyl-sn-glycero-3-phosphocholine) as a co-formulant, instead of DSPC, do not formulate phase-separated liposomes and do not target bECs.[13] It was therefore interesting to assess the significance of saturated DSPC in the phase-separated liposomes. At room temperature, DSPC is a rigid phospholipid (*Tm* 55 °C) that prefers flat orientations and therefore not favoring curvature *i.e.*, spherical liposomes.[33] PAP3 liposomes are formed (above the *Tm* of all lipids, *i.e.*, 65 °C) and slowly reach room temperature, in which DSPC is in the gel-phase. We hypothesized the gel-phase of DSPC is an important factor that induces phase-separation. Indeed, cryo-TEM imaging at 45 °C < T < 65 °C reveals ~50% of liposomes are in a fluid phase and non-phase separated, indicating full mixing of lipids (**Figure S13**). Therefore, phase separationseems to be induced after DSPC is in the gel-phase (< 55 °C).

4.3 Discussion and Conclusions

In this study, we investigate the molecular details of DOaG, a DAG lipid analogue which – when co-formulated with DSPC – leads to unique phase-separated liposomes able to target endothelial cell subsets *in vivo*, and preferentially interact with TGLs *in vivo* and *in vitro*.[13,14] Through our structure-activity relationship screening we are able to show the narrow window of *in vivo* activity of phase-separated liposomes consisting of medium (C16-C18), unsaturated diacylglycerol

analogues. All DAG analogues are summarized in **Figure 6**, depicting the relationship between their chemical character, stability, morphology and *in vivo* fate of resulting liposomes. Briefly, we find that there is increasing instability in the liposome system, directly proportional to the DOaG chain length and degree of saturation. Additionally, we show that monoacylglycerol or triacylglycerol counterparts do not result in liposomes with bEC specific behavior. Therefore, diacylglycerol analogues are the only molecules with the ability to phase-separate in membranes and result in liposomes targeting bECs in zebrafish embryos. Importantly, we show the naturally occurring DAG equivalent has the same ability to form phase-separated liposomes (although in a lower percentage within the liposome population) and target bECs in zebrafish embryos. This gives strength to the basis of our background knowledge for the DOaG lipid, as it correlates with supporting previous studies of DAG properties in lipid membranes.[25,26,29,34]

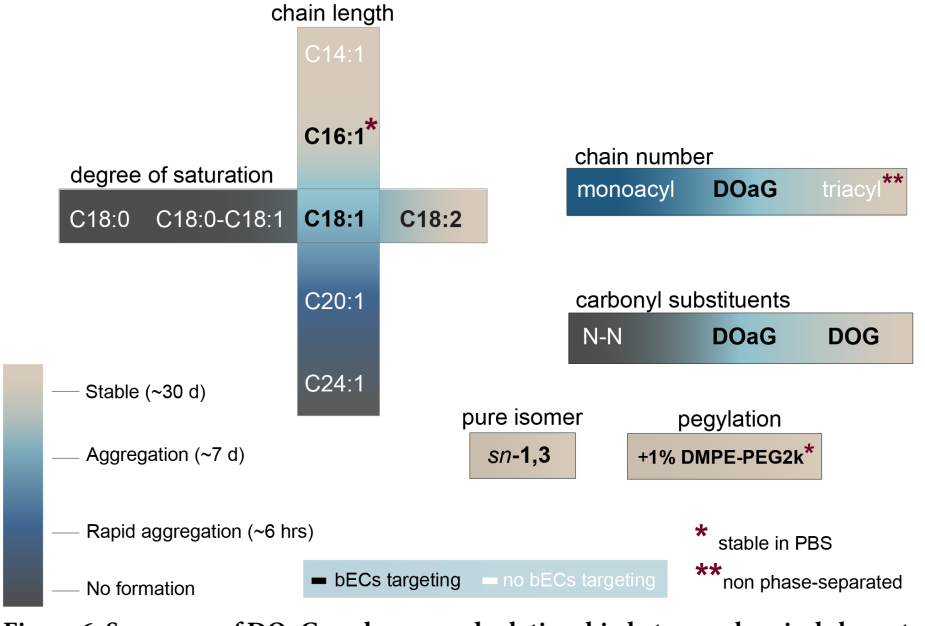

Figure 6. Summary of DOaG analogues and relationship between chemical character and stability, morphology, and *in vivo* behavior of resulting liposomes. Stability: stable for ~30 days (beige), aggregation after ~7 days (light blue), rapid aggregation after ~6 hours (dark blue), no formation (dark grey). Analogues which result in liposomes targeting bECs are written in black letters and not targeting bECs in white letters. * Stable in PBS, **Non phase-separated.

Interestingly, we find phase-separated liposomes that do not target bECs (*i.e.*, **C14:1**). We hypothesize that lipid droplets may not be the only liposome part responsible for bEC targeting, but also all parts of the bilayer which have packing defects, exposing the DOaG analogue. Excess **C14:1** accumulates in the lipid droplet – which may indeed have high packing defects – but other parts of the bilayer may be unaffected due to its shorter chains. Liposomes therefore with only a fraction of their bilayer being defected, may not have the same chance to expose DOaG analogues and be recognized and taken up by bECs, compared to liposomes with high packing defects throughout the bilayer (*i.e.*, **C16:1**, **C18:1**).

Additionally, we observe better long-term stability of liposomes containing the pure *sn*-1,3 positional isomer. The importance and effect of pure lipid isomers in lipid-based nanoparticle properties has been recently reported[35,36] and is an aspect to be considered in their development. Next, we find that liposomes consisting of the **C16:1** variant are overall more stable in PBS than the **C18:1** counterpart (DOaG) and that PEGylation of PAP3 liposomes (1 % mol DMPE-PEG2k) increases the long-term stability even further, while phase separationand bECs targeting is retained. Herein, we display a selection of DOaG analogues co-formulated with DSPC. Combinations of DOaG analogues, DAGs, and co-formulants are virtually endless, nevertheless out of the scope of this study. This work is an effort to comprehend the overall properties of a highly unusual liposome with a specific *in vivo* behavior. Lacking any 'active' targeting ligands, these liposomes depend solely on composition and morphology which dictate the nano-bio interactions. Therefore, this compositionally simple system can offer new perspectives in the design of 'targeted' liposome formulations. This work also highlights the importance of lipid composition in lipid-based nanoparticles, as even the smallest molecular changes in lipid components can greatly affect their macromolecular assembly and *in vivo* behavior.

Finally, diacylglycerols are lipids that have unique properties in lipid membranes. From membrane alteration and phase transitions, to signaling and protein recruitment, these lipids can be proven to be interesting lipid components in lipid-based nanoparticles. They could contribute to novel formulations with unique properties and functions, such as *in vivo* specificity, nanoparticle-protein communication, fusion and enhanced endosomal escape.

4.4 Materials and Methods

General reagents: 1,2-distearoyl-*sn*-glycero-3-phosphocholine (DSPC), 1,2-dioleoyl-*sn*-glycero-3-phosphoethanolamine-N-(lissamine rhodamine B sulfonyl) (DOPE-LR), were purchased from Avanti Polar Lipids (Alabaster, AL, US). Additional DSPC was purchased from Lipoid GmbH. All other chemical reagents were purchased at the highest grade available from Sigma Aldrich and used without further purification. All solvents were purchased from Biosolve Ltd. Ultrapure MilliQ® water, purified by a H_2O Advantage A10 water purification system from MilliPore, was used throughout.

Liposome formulation: Liposomes were formulated by extrusion in ddH_2O at a total lipid concentration of 5 mM, except for the PBS studies for which they were formulated in PBS. Individual lipids as stock solutions (1-10 mM) in chloroform, were combined to the desired molar ratios and dried to a thin film, first under N_2 stream, then >1 h under vacuum. The fluorescent reporter DOPE-LR (1,2-dioleoyl-*sn*-glycero-3-phosphoethanolamine-N-(lissamine rhodamine B sulfonyl) was also added in the lipid film at 0.2% moL. Lipid films were hydrated with 1mL ddH_2O (or PBS) above the T*m* of all lipids (65 °C), with gentle vortexing if necessary, to form a suspension. Large unilamellar vesicles were formed through extrusion (mini extruder, Avanti Polar Lipids) above the T*m* of all lipids (*i.e.* 65 °C). Hydrated lipids were passed 11 times through 2 x 400 nm polycarbonate (PC) membranes (Nucleopore Track-Etch membranes, Whatman), followed by 11 times through 2 x 100 nm PC membranes. All liposomes were freshly made for cryo-TEM imaging and intravenous administration in zebrafish embryos. Subsequently, all formulations were stored at 4 °C for a period of 30 days measuring their size and PDI occasionally.

Hydrodynamic diameter and PDI measurements: The hydrodynamic diameter and PDI of liposomes were obtained by using a Malvern Zetasizer Nano ZS. DLS measurements (operating wavelength = 633 nm), were carried out at room temperature in water at a total lipid concentration of approx. 100 μM. All reported DLS measurements are the average of three measurements.

Zeta potential measurements: Zeta potential of each formulation was measured at 500 μM total lipid concentration, using a dip-cell electrode (Malvern), at room

temperature. For liposomes formulated in water, aq. NaCl was added to the liposome solution prior to the measurement, to a final concentration of 10 mM. Total NaCl concentration was <20 mM for all measurements.

Cryogenic transmission electron microscopy: Liposomes (3 µL, 5 mM total lipid concentration) were applied to a freshly glow-discharged carbon 200 mesh Cu grid (Lacey carbon film, Electron Microscopy Sciences, Aurion, Wageningen, The Netherlands). Grids were blotted for 3 s at 99% humidity in a Vitrobot plunge-freezer (FEI VitrobotTM Mark III, Thermo Fisher Scientific). For PAP3 liposomes imaged at 45 ºC < T < 65 ºC , liposomes were prepared by extrusion at 65 ºC and immediately transferred in a thermomixer with a stable temperature at 65 ºC, without allowing the liposomes to reach room temperature at all times. Subsequently, liposomes were transferred in the plunge-freezer operating at 45 ºC and immediately vitrified. Cryo-TEM images were collected on a Talos L120C (NeCEN, Leiden University) or a Titan (TU Eindhoven) operating at 120 kV or 300kV, respectively. Images acquired on the Talos microscope were recorded manually at a nominal magnification of 13500x or 22000x yielding a pixel size at the specimen of 7.44 or 4.40 ångström (Å), respectively. Images acquired on the KRIOS microscope were recorded manually at a nominal magnification of 6500x or 24000x yielding a pixel size at the specimen of 13.99 or 3.87 ångström (Å), respectively.

Cryo-TEM quantification: Software Fiji (ImageJ) was used for image processing and quantification. One or more low magnification images were used to visualize at least 100 nanoparticles. Particles were counted and divided into categories (lamellar, multilamellar, phase separated, solid particles), according to their morphology. Liposomes whose morphology was not able to be identified were marked as "unidentifiable" and the number obtained was used as standard deviation for the rest of population. Liposomes that were observed to be on top or in close contact with the copper grid or overlapping with each other were excluded from the quantification.

Zebrafish husbandry and injections: Zebrafish (*Danio rerio*, strain AB/TL) were maintained and handled according to the guidelines from the Zebrafish Model Organism Database (http://zfin.org) and in compliance with the directives of the local animal welfare committee of Leiden University. Fertilization was performed by natural spawning at the beginning of the light period, and eggs were raised at 28.5

°C in egg water (60 ug/ mL Instant Ocean sea salts). The previously established zebrafish line Tg*(kdrl:*eGFP*)*^{s843} was used throughout this study.[37] Liposomes were injected into zebrafish embryos (78 hours post fertilization) using a modified microangiography protocol.[38] Embryos were anesthetized in 0.01% tricaine and embedded in 0.4% agarose containing tricaine before injection. To improve reproducibility of microangiography experiments, 1 nL injection volume was calibrated before liposomes were injected into the sinus venosus/Duct of Cuvier. A small injection space was created by penetrating the skin with the injection needle and gently pulling the needle back, thereby creating a small pyramidal space in which the liposomes were injected. Successfully injected embryos were identified through the backward translocation of venous erythrocytes and the absence of damage to the yolk ball. Injection in zebrafish embryos and imaging of biodistribution of each formulation was conducted more than once to obtain n>1. Each time freshly made liposomes were prepared.

Confocal imaging acquisition and editing: Zebrafish embryos were randomly picked from a dish of 20-60 successfully injected embryos. Confocal z-stacks were captured on a Leica TCS SPE or SP8 confocal microscope, using a 10x air objective (HCX PL FLUOTAR), a 40x water-immersion objective (HCX APO L) or 63x water-immersion objective (HC PL APO CS). For whole-embryo views, 3 overlapping z-stacks were captured to cover the complete embryo. Laser intensity, gain and offset settings were identical between stacks and experiments. Images were processed using the Fiji distribution of ImageJ. Confocal image stacks (raw data) are available upon request.

Synthesis and characterization of DAG analogues: Column Chromatography was performed using silica gel (40-63 μm, 60 Å, Screening Devices, The Netherlands). TLC analysis was performed on Merck silica gel 60/Kieselguhr F254, 0.25 mm TLC plates and compounds were visualized using a $KMnO_4$ stain (10 mg/ml $KMnO_4$ and 75 mg/ml K_2CO_3 in H_2O). ^1H spectra were recorded on a Bruker AV 400 MHz spectrometer. Chemical shifts are reported in ppm (δ), relative to the deuterated solvent as internal standard. Data are reported as follows: chemical shifts (δ), multiplets (s = singlet, d = doublet, dd = doublet of doublets, td = triplet of doublets, t = triplet, q = quartet, m = multiplet), coupling constants (J) reported in Hz.

High resolution mass spectra (HRMS) were recorded by direct injection (2 µL of a 1 µM solution in methanol) using a mass spectrometer (Q-Exactive HF Orbitrap) with an electrospray ion source (ESI) run in positive mode (source voltage 3.5 kV, capillary temperature 275 °C, no sheath gas), and with a resolution R = 240000 at m/z = 400 (mass range m/z = 160-2000). Eluents used: MeCN:H_2O (1:1 v/v) supplemented with 0,1% formic acid. For molecules **1** and **16,** high resolution mass spectra were recorded by direct injection (2 µL of a 2 µM solution in methanol) using a mass spectrometer (Synapt G2-Si [Waters]) with an electrospray ion source (ESI-TOF) run in positive mode, with LeuEnk(m/z=556.2771) as "lock mass". Source voltage of 3.5 kV, 275 °C as temperature. Mass range m/z = 160-2000. The high-resolution mass spectrometer was calibrated prior to measurements with a calibration mixture (Thermo Finnigan).

Synthesis of DOaG and DOG lipids: DOaG (**3**) and DOG (**11**) lipids were synthesized as reported in Chapter 2 and reference [13].
All lipids (except lipids **7**, **9**, **10**, **12** and **21**) were isolated as regioisomeric mixtures: 80% isomer where acyl chains substituting the *sn*-1,3 positions of the backbone and 20% isomer where acyl chains substituting the *sn*-1,2 positions of the backbone as determined by ^{1}H NMR.

(1) C14:1; 2-hydroxy-3-((Z)-tetradec-9-enamido)propyl (Z)-tetradec-9-enoate

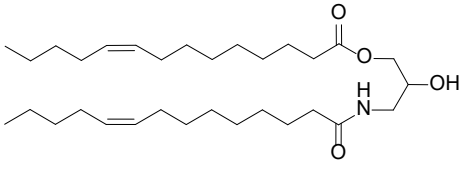

In a round bottom flask, (±)-3-amino-1,2-propane diol (10.59 mg, 0.12 mmoL), DMAP (35.51 mg, 0.29 mmoL), DIPEA (37.49 mg, 0.29 mmoL) and EDC (45.00 mg, 0.29 mmoL) were dissolved in CH_2CL_2 (10 mL). Myristoleic acid (50.00 mg, 0.22 mmoL) was added to the solution and the reaction mixture was allowed to stir overnight. The reaction mixture was washed with sat. NH_4Cl (10 mL), followed by dd. H_2O (3 x 20 mL), brine (20 mL) and subsequently was dried (with Na_2SO_4), filtered and concentrated *in vacuo*. Purification by Column Chromatography (EtOAc: hexane; graduate elution from 0:100 to 20:80) yielded compound **1** as a white solid (26.96 mg, 0.053 mmoL).

^{1}H NMR (400 MHz, $CDCl_3$) δ 6.00 (t, J = 6.0 Hz, 1H), 5.43 – 5.27 (m, 4H), 4.15 (dd, J = 11.5, 5.1 Hz, 1H), 4.05 (dd, J = 11.5, 5.8 Hz, 1H), 3.93 (qd, J = 5.8, 3.4 Hz, 1H), 3.65 – 3.46 (m, 1H), 3.23 (m, 1H), 2.33 (td, J = 7.7, 5.6 Hz, 2H), 2.27 – 2.17 (m, 2H), 2.08 – 1.96 (m, 8H), 1.62 (q, J = 7.1 Hz, 4H), 1.30 (d, J = 4.0 Hz, 24H), 0.94 – 0.81 (t, J = 8 Hz, 6H); **ESI-HRMS** (m/z) [M+H] +: calcd. for $C_{31}H_{57}NO_4$, 507.4360; found 507.4367, delta =1.4 ppm.

(2) C16:1; 3-((Z)-hexadec-9-enamido)-2-hydroxypropyl (Z)-hexadec-9-enoate

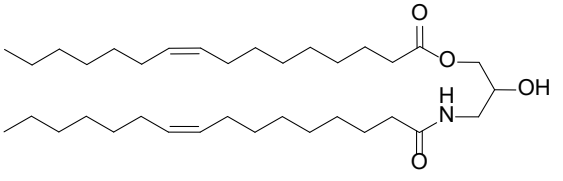

In a round bottom flask, (±)-3-amino-1,2-propane diol (100.0 mg, 1.10 mmoL), DMAP (336.0 mg, 2.75 mmoL), DIPEA (479 µL, 2.75 mmoL) and EDC (427.0 mg, 2.75 mmoL) were dissolved in CH_2Cl_2 (10 mL). Palmitoleic acid (530.5 mg, 2.10 mmoL) was added to the solution and the reaction mixture was allowed to stir overnight. The reaction mixture was washed with sat. NH_4Cl solution (10 mL), followed by dd. H_2O (3 x 10 mL), brine (10 mL) and subsequently was dried (Na_2SO_4), filtered and concentrated *in vacuo*. Purification by Column Chromatography (EtOAc : CH_2CL_2; 10:90 to 20:80) yielded compound **2** as a white solid (247.0 mg, 0.44 mmoL).

^{1}H NMR (400 MHz, $CDCl_3$) δ 6.40 (t, J = 5.8 Hz, 1H), 5.36 – 5.23 (m, 4H), 4.10 – 4.00 (m, 2H), 3.93 – 3.81 (m, 1H), 3.64 – 3.37 (m, 1H), 3.21 (dt, J = 14.1, 6.1 Hz, 1H), 2.34 – 2.24 (m, 2H), 2.17 (dd, J = 9.5, 5.8 Hz, 2H), 1.97 (q, J = 6.3 Hz, 8H), 1.58 (t, J = 7.4 Hz, 4H), 1.25 (d, J = 9.3 Hz, 32H), 0.88 – 0.80 (t, J = 8 hz, 6H). **ESI-HRMS** (m/z) $[M+H]^+$: calcd. for $C_{35}H_{65}NO_4$, 563.4986; found 563.4988, delta =0.4 ppm.

(4) C20:1; 2-hydroxy-3-((Z)-icos-11-enamido)propyl (Z)-icos-11-enoate

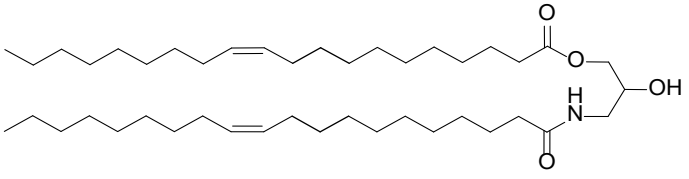

In a round bottom flask, (±)-3-amino-1,2-propane diol (7.70 mg, 0.08 mmoL), DMAP (25.66 mg, 0.21 mmoL), DIPEA (27.14mg, 0.21 mmoL) and EDC (32.60 mg, 0.21 mmoL) were dissolved in CH_2Cl_2 (10 mL). Eicosenoic acid (50 mg, 0.16 mmoL) was added to the solution and the reaction mixture was allowed to stir overnight. The reaction mixture was washed with sat. NH_4Cl solution (10 mL), followed by dd. H_2O (3 x 10 mL), brine (10 mL) and subsequently was dried (Na_2SO_4), filtered and concentrated *in vacuo*. Purification by Column Chromatography (EtOAc : CH_2CL_2; 0:100 to 20:80) yielded compound **4** as a white solid (12.00 mg, 0.02 mmoL).

^{1}H NMR (400 MHz, $CDCl_3$) δ 5.98 (t, J = 5.9 Hz, 1H), 5.39 – 5.28 (m, 4H), 4.16 (dd, J = 11.5, 5.1 Hz, 1H), 4.05 (dd, J = 11.5, 5.9 Hz, 1H), 3.94 (qd, J = 5.9, 3.4 Hz, 1H), 3.65 – 3.46 (m, 1H), 3.24 (dt, J = 14.3, 6.0 Hz, 1H), 2.40 – 2.28 (m, 2H), 2.23 (td, J = 7.6, 4.9 Hz, 2H), 2.01 (q, J = 6.0 Hz, 8H), 1.62 (q, J = 6.5, 4.9 Hz, 4H), 1.26 (d, J = 4.4 Hz, 48H), 0.90 – 0.85 (t, J = 8 hz, 6H). **ESI-HRMS** (m/z) [M+H] +: calcd. for $C_{43}H_{81}NO_4$, 676.6238; found 676.6231, delta =1.0 ppm.

(5) C24:1; 2-hydroxy-3-((Z)-tetracos-15-enamido)propyl (Z)-tetracos-15-enoate

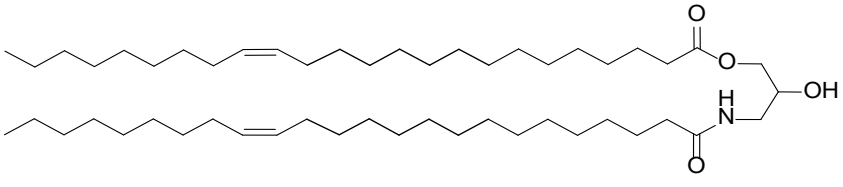

In a round bottom flask containing stirred solution of (±)-3-amino-1,2-propanediol (3.90 mg, 0.04 mmoL) in 10 mL CH_2Cl_2, nervonic acid (31.40 mg, 0.09 mmoL), DMAP (19.80 mg, 0.16 mmoL), DIPEA (13.30 mg, 0.10 mmoL) and EDC (21.84 mg, 0.14 mmoL) were added. To this solution 2 mL THF were added. The reaction mixture was allowed to stir overnight at room temperature and subsequently the mixture was washed with sat. NH_4Cl solution (10 mL), followed by dd. H_2O (3 x 10 mL), brine (10 mL). Next, the mixtrure was dried (Na_2SO_4),

filtered and concentrated *in vacuo*. Purification by Column Chromatography (CH_2Cl_2 to 20% EtOAc in CH_2Cl_2), yielded the target compound **5** (17.30 mg, 0.02 mmoL).

TLC (CH_2Cl_2:EtOAc, 8:2 v/v) : Rf = 0.26 ; **^{1}H NMR** (400 MHz, $CDCl_3$) δ 5.95 (t, J = 10.2 Hz 1H), 5.41 – 5.28 (m, 4H), 4.16 (dd, J = 11.5, 5.2 Hz, 1H), 4.05 (dd, J = 11.5, 5.9 Hz, 1H), 3.93 (dt, J = 9.1, 5.7 Hz, 1H), 3.66 – 3.48 (m, 1H), 3.27 – 3.19 (m, 1H), 2.34 (dq, J = 7.8, 5.7, 5.0 Hz, 2H), 2.22 (td, J = 7.7, 5.7 Hz, 2H), 2.01 (q, J = 6.5 Hz, 8H), 1.62 (d, J = 7.4 Hz, 4H), 1.26 (d, J = 4.0 Hz, 64H), 0.93 – 0.84 (t, J = 8 Hz, 6H). **ESI-HRMS** (m/z) [M+H]+: calcd. for $C_{51}H_{97}NO_4$, 788.7490; found 788.7485, delta = 0.7 ppm.

(6) C18:0; 2-hydroxy-3-stearamidopropyl stearate

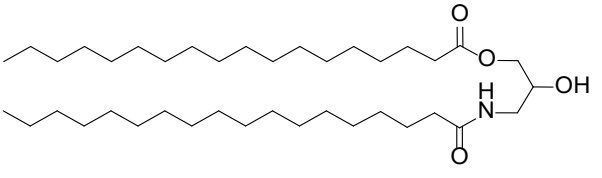

In a round bottom flask containing stirred solution of (±)-3-Amino-1,2-propanediol (100.0 mg, 1.10 mmoL) in THF (~15 mL), stearic acid (594.5 mg, 2.10 mmoL), EDCI (426.9 mg, 2.75 mmoL), DMAP (336.0 mg, 2.75 mmoL) and DIPEA (355.0 mg, 2.75 mmoL) were added. After overnight stirring at RT and subsequent evaporation of THF, the reaction mixture was diluted with $CHCl_3$, washed with sat. NH_4Cl (~15 mL) and brine (~15 mL) and subsequently was dried (Na_2SO_4), filtered *in vacuo* and concentrated. Purification by Column Chromatography (CH_2Cl_2 to 20% EtOAC in CH_2Cl_2) yielded the target material **6**.

R_f: 0.4 (CH_2Cl_2: EtOAc_8:2), **^{1}H NMR** (400 MHz, $CDCl_3$) δ 5.94 (t, J = 8 Hz 1H), 4.16 (dd, J = 11.5, 5.2 Hz, 1H), 4.05 (dd, J = 11.5, 5.8 Hz, 1H), 3.93 (qd, J = 5.7, 3.3 Hz, 1H), 3.56 (m, 1H), 3.23 (dt, J = 14.3, 5.9 Hz, 1H), 2.34 (t, J = 7.6 Hz, 2H), 2.26 – 2.18 (m, 2H), 1.62 (s, 4H), 1.25 (s, 56H), 0.91 – 0.84 (t, J = 8 Hz, 6H).

(8) C18:2; 2-hydroxy-3-((9Z,12Z)-octadeca-9,12-dienamido)propyl (9Z,12Z)-octadeca-9,12-dienoate

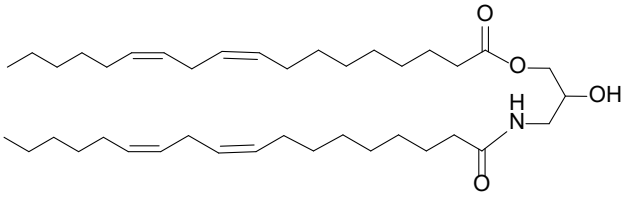

In a round bottom flask containing stirred solution of (+-)-3-amino-1,2-propanediol (54.50 mg, 0.60 mmoL) in 50 mL CH_2Cl_2, linoleic acid (336.5 mg, 1.20 mmoL), DMAP (205.1 mg, 1.68 mmoL), DIPEA (191.3 mg, 1.48 mmoL) and EDC (280.2 mg, 1.80 mmoL) were added. Next, 10 mL THF was added to the solution so that the solvent mixture was in a CH_2Cl_2:THF (5:1) ratio. The reaction mixture was stirred overnight at RT, then it was washed with saturated NH_4Cl solution and brine, and the organic phase was dried with Na_2SO_4, filtered *in vacuo*, and concentrated under reduced pressure. Purification by Column Chromatography (CH_2Cl_2 to 40% EtOAc in CH_2Cl_2) yielded the target compound **8** as a white solid (29.40 mg, 0.05 mmoL).

TLC (CH_2Cl_2:EtOAc, 8:2 v/v) : Rf = 0.45 ; **^{1}H NMR** (400 MHz, $CDCl_3$) δ 6.09 (t, J = 6 Hz, 1H), 5.43 – 5.25 (m, 8H), 4.13 (dd, J = 11.5, 5.1 Hz, 1H), 4.05 (dd, J = 11.5, 5.7 Hz, 1H), 3.92 (qd, J = 5.7, 3.3 Hz, 1H), 3.65 – 3.46 (m, 1H), 3.23 (dt, J = 14.2, 5.9 Hz, 1H), 2.76 (t, J = 6.6 Hz, 4H), 2.37 – 2.27 (m, 2H), 2.21 (td, J = 7.6, 4.8 Hz, 2H), 2.04 (q, J = 6.9 Hz, 8H), 1.61 (dq, J = 11.2, 7.1, 6.3 Hz, 4H), 1.38 – 1.22 (m, 28H), 0.90 – 0.85 (t, J = 8 Hz, 6H) ; **ESI-HRMS** (m/z) [M+H]+: calcd. for $C_{39}H_{69}NO_4$, 616.5299; found 616.5299, delta = 0.1 ppm.

(9) monoacyl; N-(2,3-dihydroxypropyl)oleamide

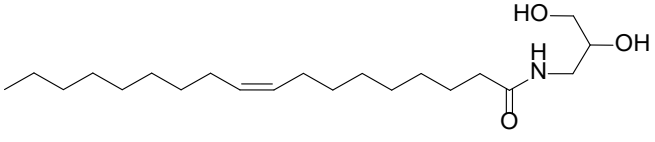

In a round bottom flask containing stirred solution of (±)-3-Amino-1,2-propanediol (200.0 mg, 2.20 mmoL) in CH_2Cl_2:THF (5:1) (50 mL), oleic acid (496.0 mg, 1.76 mmoL), EDC (402.0 mg, 2.60 mmoL), DMAP (268.0 mg, 2.20 mmoL) and DIPEA (284.0 mg, 2.20 mmoL) were added. After overnight stirring at RT and subsequent evaporation of CH_2Cl_2 and THF, the reaction mixture was diluted with $CHCl_3$, washed with sat. NH_4Cl (~25 mL) and brine (~25 mL) and subsequently was dried (Na_2SO_4), filtered in vacuo and concentrated, so the

crude compound was obtained. Purification by Column Chromatography (CH_2Cl_2 to 50% EtOAc in CH_2Cl_2) yielded the target material **9** as a white solid (469.3 mg, 1.32 mmoL).

^{1}H NMR (400 MHz, $CDCl_3$) δ 6.22 (t, J = 6.1 Hz, 1H), 5.42 – 5.26 (m, 2H), 3.75 (t, J = 4.9 Hz, 1H), 3.64 – 3.49 (m, 4H), 3.39 (m, 2H), 2.25 – 2.17 (m, 2H), 2.00 (q, J = 6.4 Hz, 4H), 1.61 (t, J = 7.4 Hz, 2H), 1.27 (d, J = 12.0 Hz, 20H), 0.94 – 0.83 (t, J = 8.0 Hz, 3H). **ESI-HRMS** (m/z) [M+H]+: calcd. for $C_{21}H_{41}NO_3$, 355.3159; found 355.3158, delta = 0.3 ppm.

(10) triacyl; 3-oleamidopropane-1,2-diyl dioleate

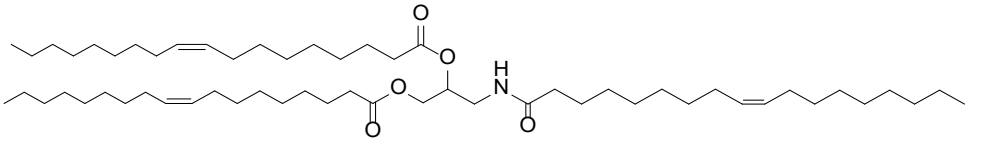

In a round bottom flask containing stirred solution of (±)-3-Amino-1,2-propanediol (92.00 mg, 1.01 mmoL) in CH_2Cl_2 (25 mL), oleic acid (1.0 g, 3.54 mmoL), HCTU (2.0 g, 5.26 mmoL) and DIPEA (1.3 g, 10.23 mmoL) were added. After overnight stirring at RT, the reaction mixture was diluted with CH_2CL_2, washed with sat. NH_4Cl (~30 mL) and brine (~30 mL) and subsequently was dried (Na_2SO_4), filtered *in vacuo* and concentrated. Purification by Column Chromatography (CH_2Cl_2 to 2% EtOAC in CH_2Cl_2) yielded the target material **10** as a white solid (193.0 mg, 0.22 mmoL).

TLC (CH_2Cl_2: EtOAc_8:2) : R_f = 0.9, **^{1}H-NMR** ($CDCl_3$, 400MHz) δ 5.73 (t, J = 5.8 Hz, 1H), 5.39 – 5.27 (m, 6H), 5.09 (m, 1H), 4.25 (dd, J = 12.0, 4.1 Hz, 1H), 4.13 (dd, J = 12.0, 5.7 Hz, 1H), 3.48 (m, 2H), 2.31 (td, J = 7.6, 2.2 Hz, 4H), 2.16 (t, J = 7.6 Hz, 2H), 2.00 (q, J = 6.3 Hz, 12H), 1.60 (s, 6H), 1.28 (d, J = 10.4 Hz, 62H), 0.88 (t, J = 6.8 Hz, 9H); **ESI-HRMS** (m/z) [M+H]+: calcd. for $C_{57}H_{105}NO_5$, 884.8066; found 884.8062, delta = 0.5 ppm.

(12)N-N,(9Z,9'Z)-1,1'-((2-hydroxypropane-1,3-diyl)bis(l2-azanediyl)) bis(octadec-9-en-1-one)

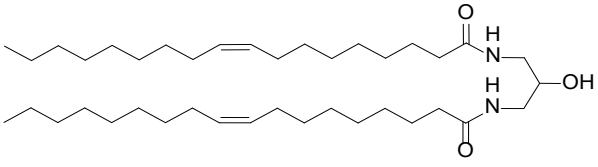

In a round bottom flask containing a stirred solution of 1,3-diamino-2-propanol (102.4 mg, 1.12 mmoL) and oleic acid (595.2 mg, 2.11 mmoL), DMAP (356.9 mg, 2.92 mmoL), EDC (437.1 mg, 2.82 mmoL) and DIPEA (356.7 mg, 2.76 mmoL) were added. The mixture was diluted with 10 mL of CH_2Cl_2 and 3 mL of THF. After stirring overnight at RT, the reaction mixture was diluted with CH_2Cl_2 before washing with saturated NH_4Cl (2x ~15 mL), and brine (~15 mL). Subsequently, the mixture was dried with Na_2SO_4 and filtered *in vacuo* and concentrated. Purification by Column Chromatography (CH_2Cl_2 to 50% EtOAc in CH_2Cl_2), yielded the target material **12** as a white solid (274.5 mg, 0.44 mmoL).

^{1}H NMR (400 MHz, $CDCl_3$) δ 6.79 (t, J = 6.3 Hz, 2H), 5.38 – 5.30 (m, 4H), 3.74 (m, 1H), 3.38 (m, 2H), 3.21 (dt, J = 14.0, 5.5 Hz, 2H), 2.24 – 2.15 (m, 4H), 1.99 (q, J = 6.6 Hz, 8H), 1.60 (m, 4H), 1.26 (d, J = 13.1 Hz, 40H), 0.90 – 0.82 (t, J = 8 Hz, 6H).
ESI-HRMS (m/z) $[M+H]^+$: calcd. for $C_{39}H_{69}NO_4$, 619.5772; found 619.5771, delta = 0.2 ppm.

Synthetic route for lipids 7 and 21. Each *sn*-position of the amino-propanediol was first coupled to a protecting group (PG) in 3 synthetic steps, leading to a full protected amino-propanediol with PG1, PG2 and PG3 protecting the -NH_2 of *sn*-1 position, -OH of the *sn*-3 position and the -OH of the *sn*-2 position, respectively (**Figure S15**). All protecting groups were orthogonal with each other. Synthesis steps: 1) Deprotection of the NH group, 2) subsequent coupling with fatty acid (oleic acid) in *sn*-1 position, 3) deprotection of OH group in *sn*-3 position, 4) subsequent coupling with fatty acid (stearic acid for **7** or oleic acid for **21**) in *sn*-3 position, 5) deprotection of OH group in *sn*-2 position.

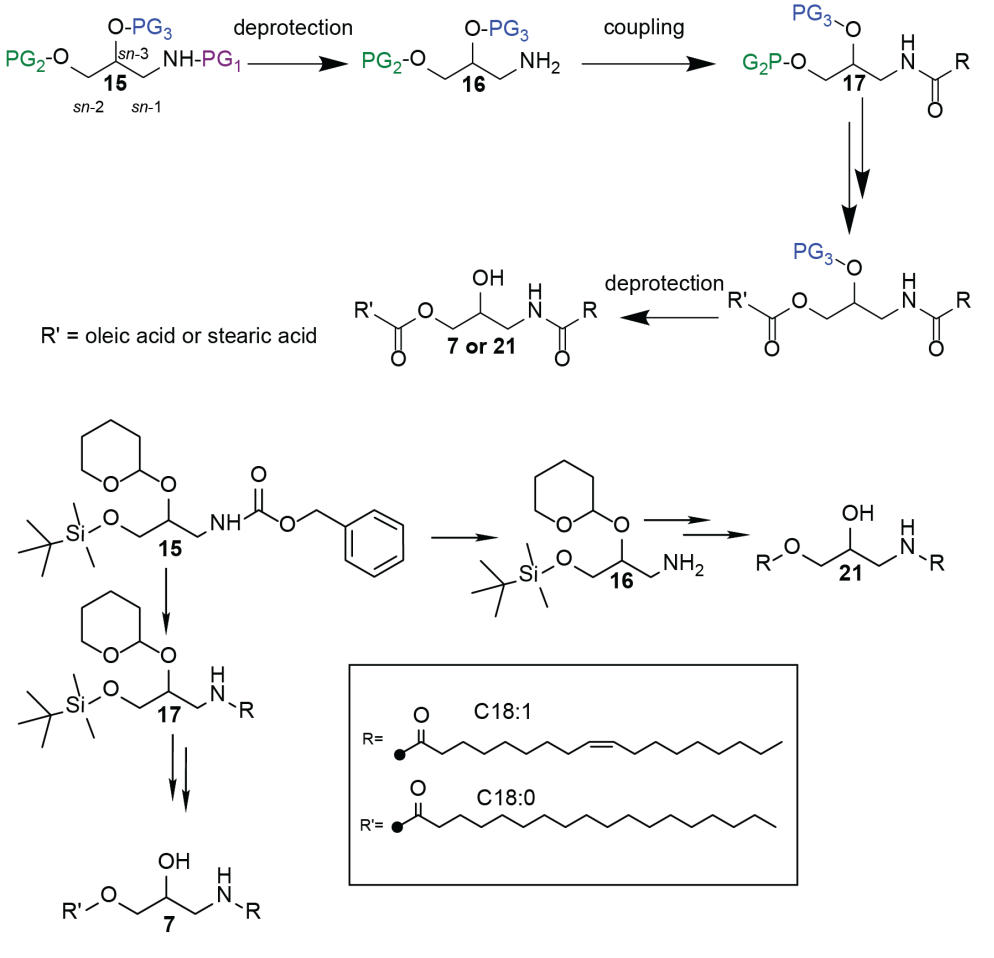

Figure S15. Schematic of synthetic route for lipids 7 and 21.

(13) Benzyl (2,3-dihydroxypropyl) carbamate

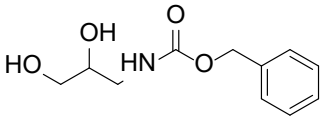

In a round bottom flask, 3-amino-1,2-propane diol (1.5 g, 16.6 mmol) was dissolved in THF (50 mL). Water (25 mL) and potassium carbonate (6.9 g; 49.7 mmol) were added to the solution and the reaction mixture was cooled down to 0 °C. Benzyl chloroformate (3.8 g, 16.5 mmol) was added dropwise over 2 hours and afterwards was allowed to warm to room temperature and left stirring overnight. The reaction mixture was extracted with EtOAc (3 x 25 mL), the combined organic layers were washed with brine (20 mL) and subsequently was dried (Na_2SO_4), filtered and concentrated *in vacuo*. Purification by Column Chromatography (MeOH: CH_2Cl_2; graduate elution from 0:100 to 6:94 in steps of 2%) yielded the title compound **13** as a white solid (3.47 g, 15.4 mmol).

^{1}H NMR (400 MHz, MeOD) δ 7.37 – 7.23 (m, 5H), 5.06 (s, 2H), 3.66 (dq, J = 7.1, 5.1 Hz, 1H), 3.47 (tt, J = 11.4, 6.3 Hz, 2H), 3.29 – 3.21 (m, 1H), 3.12 (dd, J = 13.8, 6.8 Hz, 1H).

(14) Benzyl (3-((tert-butyldimethylsilyl)oxy)-2-hydroxypropyl)carbamate

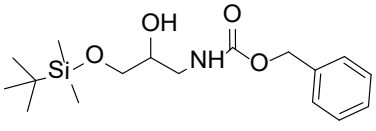

In a 500 mL round bottom flask compound **13** (3.1 g; 13.9 mmol) was dissolved in CH_2Cl_2 (30 mL). Imidazole (2.4 g, 34.7 mmol) was added to the solution and the reaction mixture was cooled down to 0 °C. TBDMS-Cl (3.1 g, 20.8 mmol) was added and the reaction mixture was allowed to stir for 2 hours while maintaining 0 °C. The reaction mixture was quenched with sat. $NaHCO_3$ solution (25 mL) and washed with dd. H_2O (3 x 10 mL) and subsequently was dried (Na_2SO_4), filtered and concentrated *in vacuo*. Purification by Column Chromatography (EtOAc: petroleum ether; 10:90 to 25:75) yielded the title compound **14** as a colorless oil (3.83 g, 11.0 mmol).

^{1}H NMR (400 MHz, MeOD) δ 7.39 – 7.24 (m, 5H), 6.85 (d, J = 5.9 Hz, 1H), 5.07 (s, 2H), 3.70 (dt, J = 10.6, 5.1 Hz, 1H), 3.65 – 3.54 (m, 2H), 3.40 – 3.29 (m, 1H), 3.20 – 3.08 (m, 1H), 0.92 (s, 9H), 0.08 (s, 6H).

(15) Benzyl (3-((tert-butyldimethylsilyl)oxy)-2-((tetrahydro-2H-pyran-2-yl)oxy)propyl) carbamate

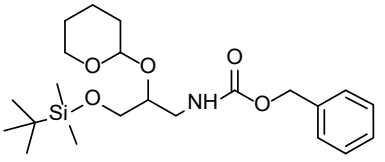

In a round bottom flask, compound **14** (2.9 g, 8.65 mmoL) was dissolved in CH_2Cl_2 alongside pyridinium p-toluenesulfonate (0.22 g, 0.884 mmoL). 3,4-dihydro-pyran (2.2 g, 25.95 mmoL) was added and the reaction was allowed to stir for 3 hours. The reaction mixture was washed with sat. $NaHCO_3$ solution (25 mL), followed by H_2O (2 x 25 mL) and brine (25 mL) and subsequently was dried (Na_2SO_4), filtered and concentrated *in vacuo*. Purification by Column Chromatography (EtOAc: hexane; graduate elution from 1:99 to 10:90 in steps of 1%, followed by a flush of 50:50) yielded the title compound **15** as a colorless oil (3.14 g, 7.40 mmoL).

^{1}H NMR (400 MHz, $CDCl_3$) δ 7.42 – 6.99 (m, 5H), 5.80 – 5.45 (m, 1H), 5.03 (s, 2H), 4.71 – 4.52 (m, 1H), 3.84 (dt, J = 10.5, 4.7 Hz, 1H), 3.73 (dq, J = 16.1, 5.3, 4.9 Hz, 1H), 3.57 (dd, J = 12.9, 4.5 Hz, 1H), 3.50 – 3.33 (m, 2H), 3.29 – 3.08 (m, 1H), 1.83 – 1.56 (m, 2H), 1.51 – 1.36 (m, 4H), 0.86 (s, 9H), 0.02 (d, J = 6.1 Hz, 6H).

(16)3-((tert-butyldimethylsilyl)oxy)-2-((tetrahydro-2H-pyran-2-yl)oxy)propan-1-amine

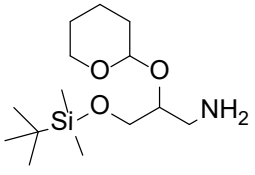

Compound **15** (1.9 g, 4.50 mmoL) was dried in a round bottom flask before use in a vacuum oven (25 °C) for at least 2 hours. Palladium on carbon (191.0 mg) was added and the round bottom flask was flushed with nitrogen gas for 10 minutes. Dry MeOH was added, and to the stirred solution with addition of a nitrogen balloon, triethylsilane (7.9 g, 67.6 mmoL) was added dropwise. The reaction mixture was allowed to stir for 4 hours and then was filtered over Celite, cleansed with MeOH and concentrated *in vacuo*. Excess of triethylsilane was removed under airflow for 30 min. Purification by Column Chromatography (CH_2Cl_2 + 0,5 % isopropylamine with graduate elution to 2.5 % EtOH in CH_2Cl_2 + 0.5 % isopropylamine in steps of 0.5% EtOH) yielded the title compound **16** as a colorless oil (1.16 g, 4.00 mmoL).

^{1}H NMR (400 MHz, $CDCl_3$) δ 4.61 (td, J = 5.7, 5.1, 2.7 Hz, 1H), 3.83 (m, 1H), 3.77 – 3.70 (m, 1H), 3.63 – 3.45 (m, 2H), 3.44 – 3.34 (m, 1H), 2.80 (m, 1H), 2.65 (m, 1H), 1.80 – 1.57 (m, 2H), 1.53 – 1.36 (m, 4H), 1.28 (s, 2H), 0.79 (s, 9H), -0.05 (d, J = 3.2 Hz, 6H). **ESI-HRMS** (m/z) [M+H]+: calcd. for $C_{14}H_{31}NO_3Si$, 289.2146; found 289.2154, delta=2.8 ppm.

(17)N-(3-((tert-butyldimethylsilyl)oxy)-2-((tetrahydro-2H-pyran-2-yl)oxy)propyl) oleamide

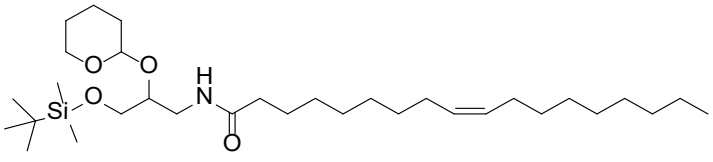

In a round bottom flask, compound **16** (915.3 mg, 3.16 mmoL), DMAP (1.0 g, 8.2 mmoL), DIPEA (1.1 g, 8.2 mmoL) and EDC (1.3 g, 8.2 mmoL) were dissolved in CH_2Cl_2 (20 mL). Oleic acid (1.3 g, 4.74 mmoL) was added to the solution and the reaction mixture was allowed to stir at RT overnight. The reaction mixture was washed with sat. NH_4Cl solution (20 mL), followed by H_2O (3 x 20 mL), brine (20 mL) and subsequently was dried (Na_2SO_4), filtered and concentrated *in vacuo*. Purification by Column Chromatography (EtOAc: hexane; graduate elution from 0:100 to 20:80 in steps of 10%) yielded the title compound **17** as a colorless oil (1.30 g, 2.35 mmoL).

^{1}H NMR (400 MHz, $CDCl_3$) δ 6.67 – 6.01 (m, 1H), 5.38 – 5.25 (m, 2H), 4.62 (m, 1H), 4.00 – 3.83 (m, 1H), 3.83 – 3.67 (m, 2H), 3.64 (dd, J = 9.6, 6.0 Hz, 1H), 3.61 – 3.53 (m, 2H), 3.48 (m, 1H), 3.40 – 2.96 (m, 1H), 2.14 (td, J = 8.3, 6.9 Hz, 2H), 2.05 – 1.94 (m, 4H), 1.88 – 1.67 (m, 2H), 1.64 – 1.55 (m, 2H), 1.54 – 1.46 (m, 4H), 1.26 (d, J = 13.0 Hz, 20H), 0.88 (s, 9H), 0.87 – 0.82 (t, J = 4 Hz, 3H), 0.04 (dd, J = 9.8, 1.4 Hz, 6H).

(18) N-(3-hydroxy-2-((tetrahydro-2H-pyran-2-yl)oxy)propyl)oleamide

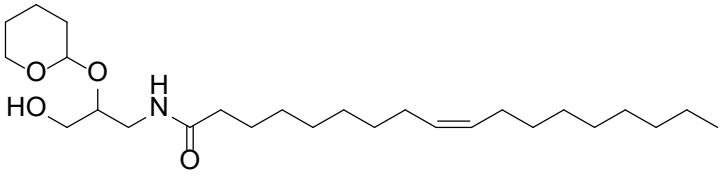

In a round bottom flask, compound **17** (1.2 g; 2.09 mmoL) was dissolved in THF (30 mL) and the reaction mixture was cooled down to 0 °C. TBAF·3 H_2O (2.0 g, 6.27 mmoL) was dissolved in a small amount of THF and was added dropwise. The mixture was allowed to stir for 1 hour. Afterwards the reaction mixture was diluted with H_2O (30 mL) extracted with EtOAc (3 x30 mL) and subsequently was dried (Na_2SO_4), filtered and concentrated *in vacuo*. Purification by Column Chromatography (EtOAc: hexane; elution from 0:100 to 50:50 in steps of 10%) yielded the title compound **18** as a colorless oil (0.78 g, 1.77 mmoL).

^{1}H NMR (400 MHz, $CDCl_3$) δ 6.09 (dt, J = 196.7, 6.1 Hz, 1H), 5.40 – 5.26 (m, 2H), 4.56 (dq, J = 6.2, 2.8 Hz, 1H), 3.95 (dq, J = 13.0, 3.6, 2.9 Hz, 1H), 3.76 (dp, J = 11.0, 5.4 Hz, 1H), 3.58 – 3.33 (m, 5H), 2.19 (q, J = 7.1 Hz, 2H), 1.99 (q, J = 6.4 Hz, 4H), 1.90 – 1.71 (m, 2H), 1.61 (t, J = 7.2 Hz, 2H), 1.58 – 1.46 (m, 4H), 1.27 (d, J = 14.6 Hz, 20H), 0.87 (t, J = 6.7 Hz, 3H).

(19) 3-oleamido-2-((tetrahydro-2H-pyran-2-yl)oxy)propyl stearate

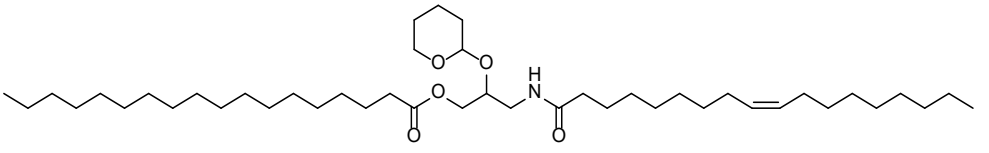

In a round bottom flask, compound **18** (322.7 mg, 0.73 mmoL), DMAP (224.2 mg, 1.83 mmoL), DIPEA (236.5 mg, 1.83 mmoL) and EDC (284.1 mg, 1.83 mmoL) were dissolved in CH_2Cl_2 (10 mL). Stearic acid (31.93 mg, 0.11 mmoL) was added to the solution and the reaction mixture was allowed to stir overnight at RT. The reaction mixture was washed with sat. NH_4Cl solution (10 mL), followed by H_2O (3 x 10 mL), brine (20 mL) and subsequently was dried (Na_2SO_4), filtered and concentrated *in vacuo*. Purification by Column Chromatography (Acetone : CH_2Cl_2, 5:95) yielded the title compound **19** as a white solid (247.2 mg, 0.35 mmoL).

^{1}H NMR (400 MHz, $CDCl_3$) δ 5.38 – 5.27 (m, 2H), 4.74 – 4.47 (m, 1H), 4.28 – 4.05 (m, 2H), 3.99 – 3.83 (m, 2H), 3.65 – 3.42 (m, 3H), 3.35 – 3.08 (m, 1H), 2.31 (q, J = 7.9 Hz, 3H), 2.21 – 2.12 (m, 2H), 1.99 (q, J = 6.8 Hz, 4H), 1.88 – 1.67 (m, 2H), 1.60 (td, J = 7.3, 3.9 Hz, 4H), 1.56 – 1.46 (m, 3H), 1.27 (d, J = 19.3 Hz, 34H), 0.90 – 0.84 (t, J = 8 Hz, 6H).

(7) C18:0-C18:1; 2-hydroxy-3-oleamidopropyl stearate

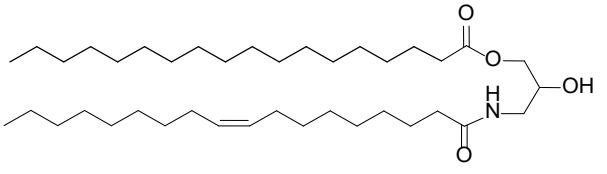

In a round bottom flask, compound **19** (223.0 mg, 0.32 mmoL) and pyridinium p-toluene sulfonate (8.04 mg, 0.032 mmoL) were dissolved in MeOH (5 mL) and the reaction mixture was allowed to stir overnight at 50 °C. The reaction mixture was quenched with sat. NaHCO3 solution (10 mL) and was extracted with EtOAc (3 x 10 mL) and subsequently was dried (Na_2SO_4), filtered and concentrated *in vacuo*. Purification by Column

Chromatography (EtOAc:CH_2Cl_2, graduate elution from 0:100 to 30:70) yielded the final compound **7** as a white solid (168.0 mg, 0.27 mmoL).

^{1}H NMR (400 MHz, $CDCl_3$) δ 6.00 (t, J = 5.9 Hz, 1H), 5.39 – 5.28 (m, 2H), 4.14 (dd, J = 11.5, 5.2 Hz, 1H), 4.05 (dd, J = 11.5, 5.8 Hz, 1H), 3.93 (qd, J = 5.7, 3.3 Hz, 1H), 3.53 (m, 1H), 3.23 (dt, J = 14.3, 6.0 Hz, 1H), 2.33 (t, J = 7.6 Hz, 2H), 2.26 – 2.17 (m, 2H), 2.00 (q, J = 6.5 Hz, 4H), 1.62 (m, 4H), 1.27 (d, J = 19.7 Hz, 48H), 0.91 – 0.83 (m, 6H); **ESI-HRMS** (m/z) [M+H]+: calcd. for $C_{39}H_{75}NO_4$, 622.5769; found 622.5767, delta = 0.5 ppm.

(20) 3-oleamido-2-((tetrahydro-2H-pyran-2-yl)oxy)propyl oleate

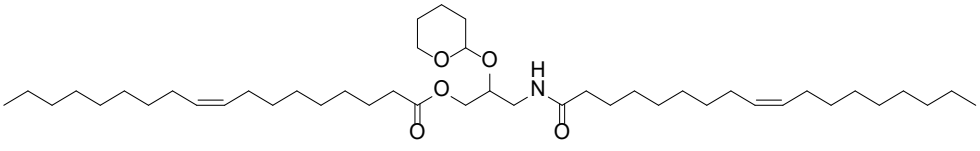

In a round bottom flask, compound **18** (295.1 mg, 0.67 mmoL), DMAP (205.0 mg, 1.68 mmoL), DIPEA (217.1 mg, 1.68 mmoL) and EDC (260.8 mg, 1.68 mmoL) were dissolved in CH_2Cl_2 (10 mL). Oleic acid (282.5 mg, 1.0 mmoL) was added to the solution and the reaction mixture was allowed to stir overnight at RT. The reaction mixture was washed with sat. NH_4Cl solution (10 mL), followed by H_2O (3 x 10 mL), brine (20 mL) and subsequently was dried (Na_2SO_4), filtered and concentrated *in vacuo*. Purification by Column Chromatography (Acetone: CH_2Cl_2, 5:95) yielded the title compound **20** as a colorless oil (308.5 mg, 0.44 mmoL).

^{1}H NMR (400 MHz, $CDCl_3$) δ 6.61 – 6.09 (m, 1H), 5.31 – 5.18 (m, 4H), 4.70 – 4.45 (m, 1H), 4.10 (m, 1H), 4.01 (dd, J = 5.5, 2.5 Hz, 1H), 3.91 – 3.76 (m, 2H), 3.54 – 3.32 (m, 2H), 3.28 – 2.95 (m, 1H), 2.23 (q, J = 7.2 Hz, 2H), 2.09 (q, J = 7.4 Hz, 2H), 1.92 (q, J = 6.4 Hz, 8H), 1.79 – 1.59 (m, 2H), 1.59 – 1.38 (m, 4H), 1.45 (dq, J = 8.6, 5.5, 5.1 Hz, 4H), 1.20 (d, J = 13.5 Hz, 40H), 0.83 – 0.75 (t, J = 8 Hz, 6H).

(21) *sn*-1,3; 2-hydroxy-3-oleamidopropyl oleate

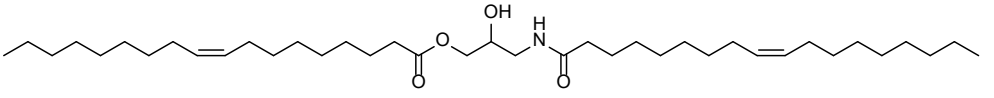

In a round bottom flask, compound **20** (269.3 mg, 0.38 mmoL) and pyridinium p-toluene sulfonate (9.50 mg, 0.038 mmoL) were dissolved in MeOH (5 mL) and the reaction mixture was allowed to stir overnight at 50 °C. The reaction mixture was quenched with sat. NaHCO3 solution (10 mL) and was extracted with EtOAc (3 x 10 mL) and subsequently was dried (Na_2SO_4), filtered and concentrated *in vacuo*. Purification by Column Chromatography (EtOAc:CH_2Cl_2, graduate elution from 0:100 to 30:70) yielded the final compound **21** as a white solid (200.2 mg, 0.32 mmoL).

^{1}H NMR (400 MHz, $CDCl_3$) δ 5.98 (t, J = 6.0 Hz, 1H), 5.40 – 5.27 (m, 4H), 4.15 (dd, J = 11.4, 5.1 Hz, 1H), 4.05 (dd, J = 11.5, 5.8 Hz, 1H), 3.93 (qd, J = 5.8, 3.3 Hz, 1H), 3.53 (m, 1H), 3.23 (dt, J = 14.2, 6.0 Hz, 1H), 2.33 (t, J = 7.6 Hz, 2H), 2.24 – 2.18 (m, 2H), 2.00 (q, J = 6.5 Hz, 8H), 1.62 (m, 1H), 1.28 (d, J = 14.3 Hz, 40H), 0.91 – 0.83 (t, J = 8 Hz, 6H); **ESI-HRMS** (m/z) [M+H]+: calcd. for $C_{39}H_{73}NO_4$, 619.5612; found 619.5610, delta = 0.3 ppm.

4.5 Supporting Figures and ^{1}H-NMR spectra

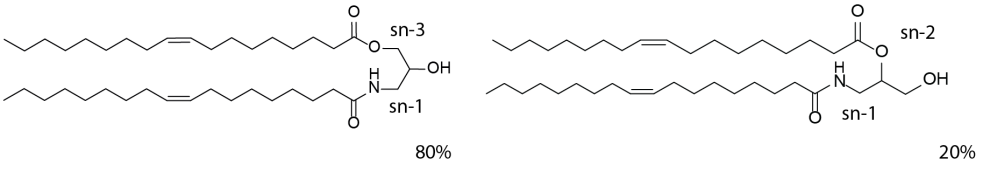

Figure S1. Positional isomers found as a mixture in DOaG lipid. Fatty acid tails substituting the *sn*-1,3 position (80%, majority) and *sn*-1,2 (20%). All lipids are also a racemic mixture.

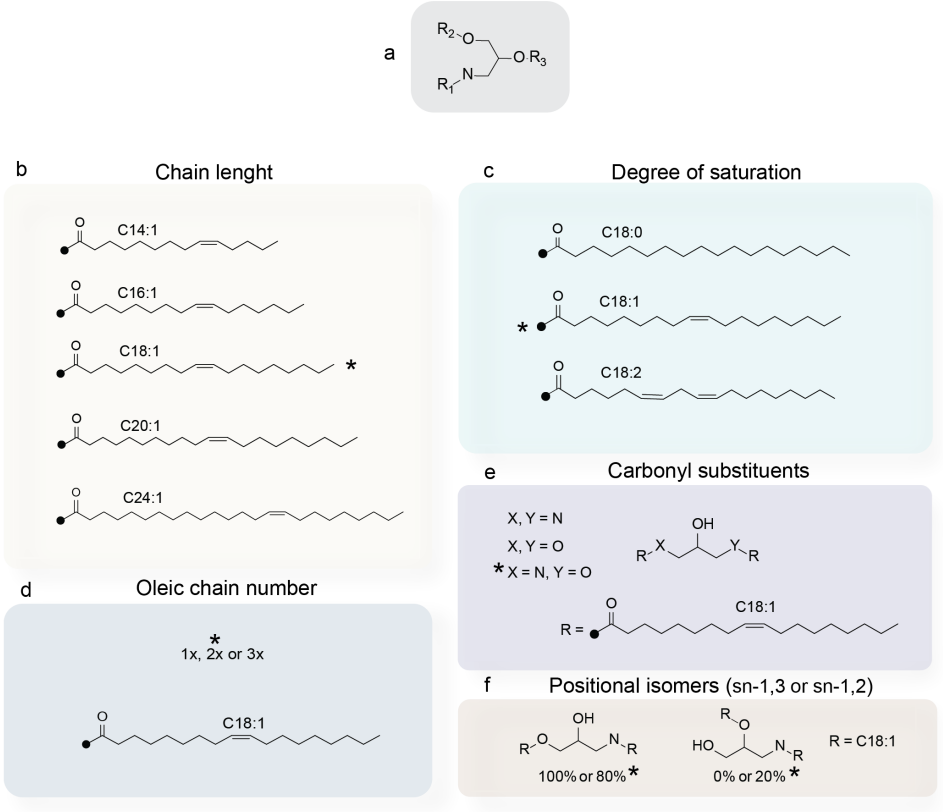

g

No.	Code	R_1	R_2	R_3	No.	Code	R_1	R_2	R_3
1	**C14:1**	C14:1	C14:1	H	8	**C18:2**	C18:2	C18:2	H
2	**C16:1**	C16:1	C16:1	H					
*3	**C18:1**	C18:1	C18:1	H	9	**Monoacyl**	C18:1	H	H
4	**C20:1**	C20:1	C20:1	H	10	**Triacyl**	C18:1	C18:1	C18:1
5	**C24:1**	C24:1	C24:1	H	11	**N-N**	C18:1	C18:1	H
6	**C18:0**	C18:0	C18:0	H	12	**DOG**	C18:1	C18:1	H
7	**C18:0-C18:1**	C18:0	C18:1	H	13	***sn*-1,3**	C18:1	H	C18:1

Figure S2. Library of DOaG analogues. a) Glycerol-like DOaG backbone. DOaG analogues varying **b)** chain length, **c)** degree of saturation, **d)** number of fatty acid tails, **e)** carbonyl substituents of the backbone, **f)** positional isomers. **g)** table depicting the number and code of each lipid and the substitution of each *sn* position of the DOaG backbone. DOaG (as a reference) is indicated with *.

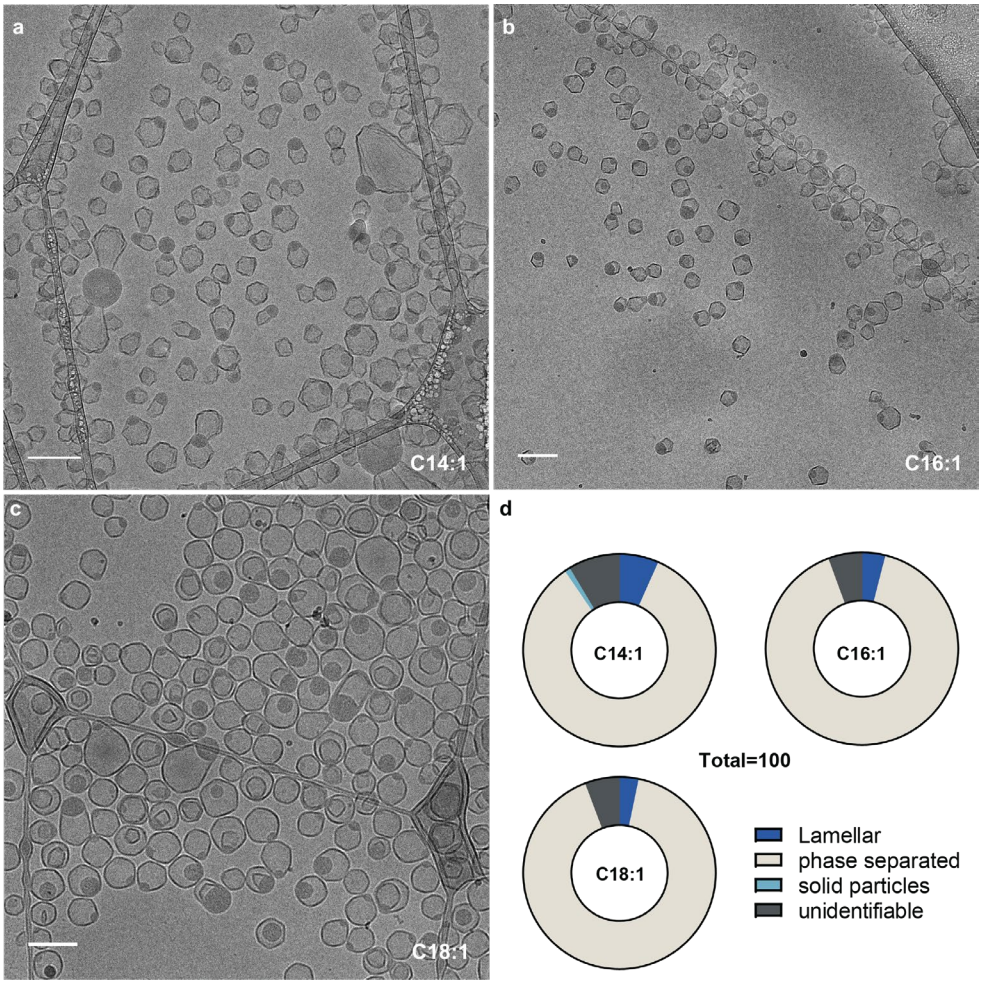

Figure S3. Cryo-TEM images of liposomes containing 1:1 molar ratio of DSPC and a) C14:1, **b)** C16:1, **c)** 18:1 (DOaG). **d)** Quantification of all populations in liposomal formulations containing 1:1 molar ratio of DSPC and C14:1, C16:1 or 18:1 (DOaG). Quantification based on cryo-TEM images a-c (N=100). Scale bars: 200 nm.

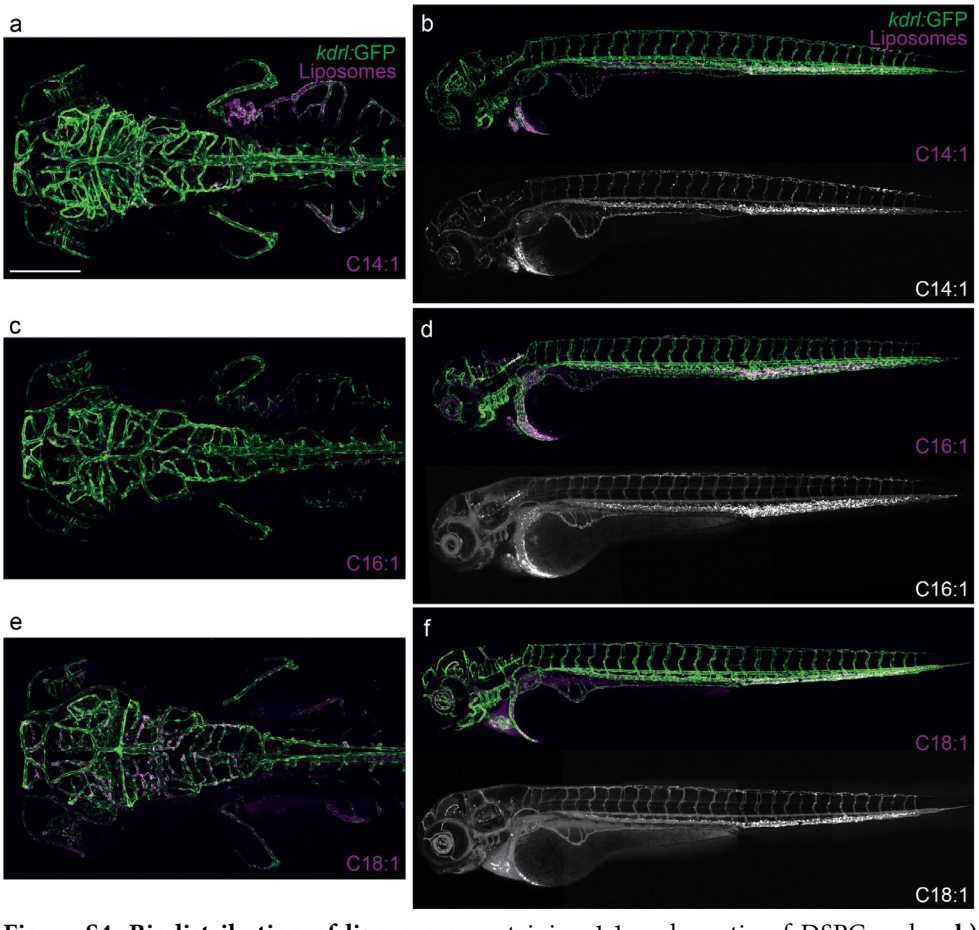

Figure S4. Biodistribution of liposomes containing 1:1 molar ratio of DSPC and **a, b)** C14:1, **c, d)** C16:1 and **e, f)** C18:1 (PAP3 liposomes) in Tg(kdrl:GPF) zebrafish embryos, expressing GFP in all endothelial cells, in dorsal (10x magnification) and lateral view, 1.5 hours post injection (hpi), at 78 days post fertilization (dpf). Liposomes in grey/magenta at 5mM total lipid concentration containing 0.2% DOPE-LR (1,2-dioleoyl-sn-glycero-3-phosphoethanolamine-N-[lissamine rhodamine B sulfonyl]) for visualization. Vasculature in green. Scale bar for a, c, e: 200 µm.

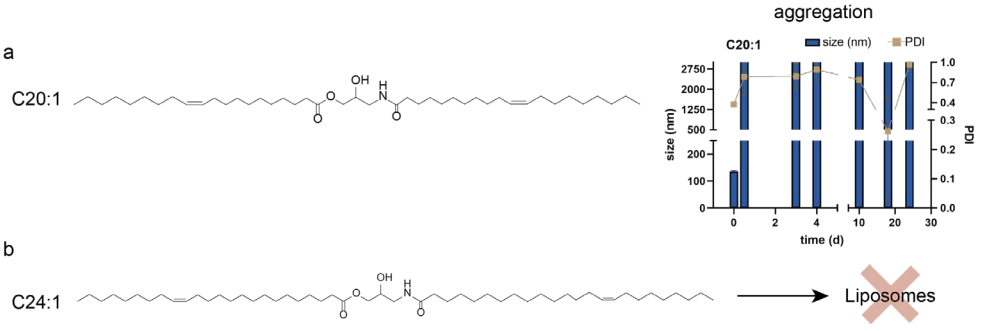

Figure S5. DOaG variants resulting in unstable formulations. a) Liposomes composed with DSPC and C20:1 variant (1:1 molar ratio) aggregate rapidly within ~6 hours as seen by size and polydispersity index (PDI) measurements (size and PDI limit of a formulation relevant for *in vivo* application = 200nm and 0.2, respectively). **b)** A mixture of DSPC and C24:1 (1:1 molar ratio) cannot be formulated into liposomes as the lipid film hydration step failed.

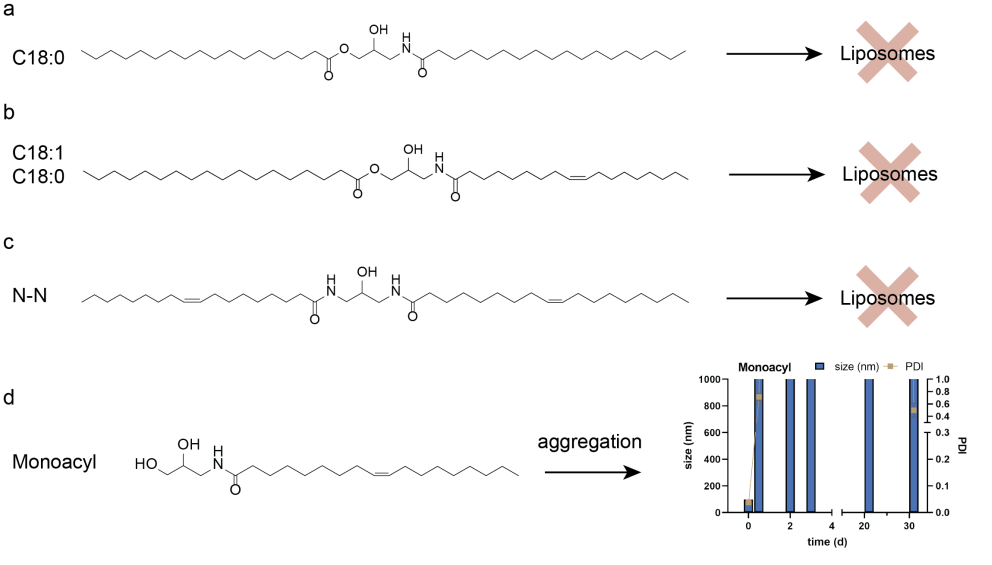

Figure S6. DOaG variants resulting in unstable formulations. Mixture of DSPC and **a)** C18:0, **b)** C18:0-C18:1 or **c)** N-N (in 1:1 molar ratio) cannot be formulated into liposomes as the lipid film hydration step failed. **d)** Liposomes composed with DSPC and monoacyl variant (1:1 ratio) aggregate rapidly within ~6 hours, as seen by size and PDI measurements (size and PDI limit of a formulation relevant for *in vivo* application = 200nm and 0.2, respectively).

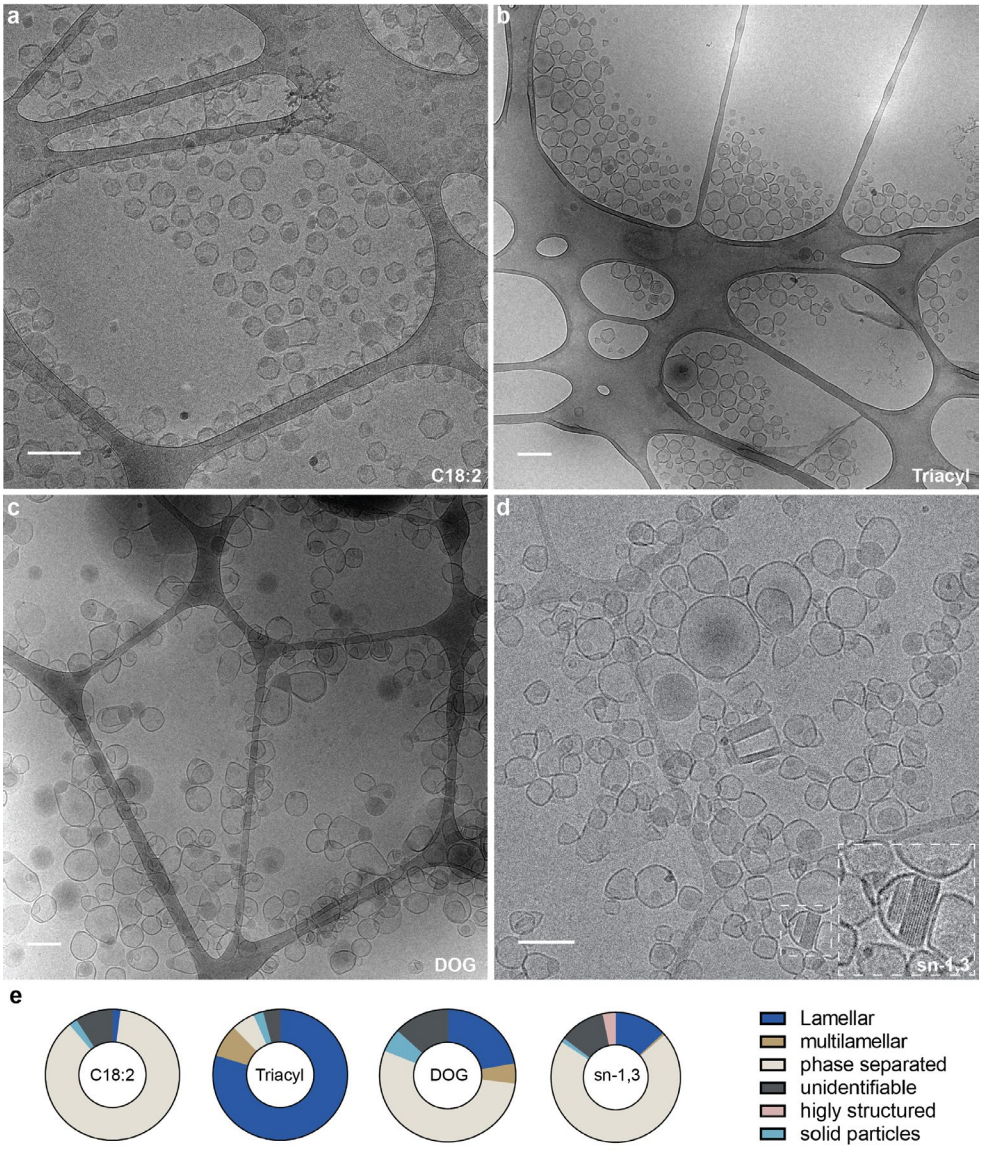

Figure S7. Cryo-TEM images of liposomes containing 1:1 molar ratio of DSPC and a) C18:2, **b)** Triacyl, **c)** DOG or **d)** *sn*-1,3. **e**) Quantification of all populations found in liposomal formulations containing 1:1 molar ratio of DSPC and C18:2, triacyl, DOG or *sn*-1,3. Inset in d depicts highly structured, crystalline assemblies present in the formulation. Quantification based on cryo-TEM images a-d (N=100). Scale bars: 200 nm.

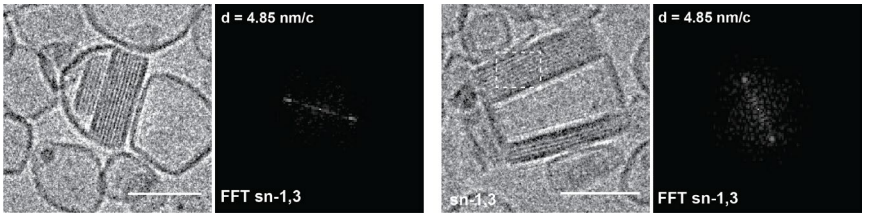

Figure S8. Liquid-crystalline assemblies as seen in *sn*-1,3 containing liposomes. Cryo-TEM images of liposomes containing the liquid-crystalline phases and average repeating distance of the lattice as indicated by FFT (nm per repeating cycle). Scale bars: 100 nm.

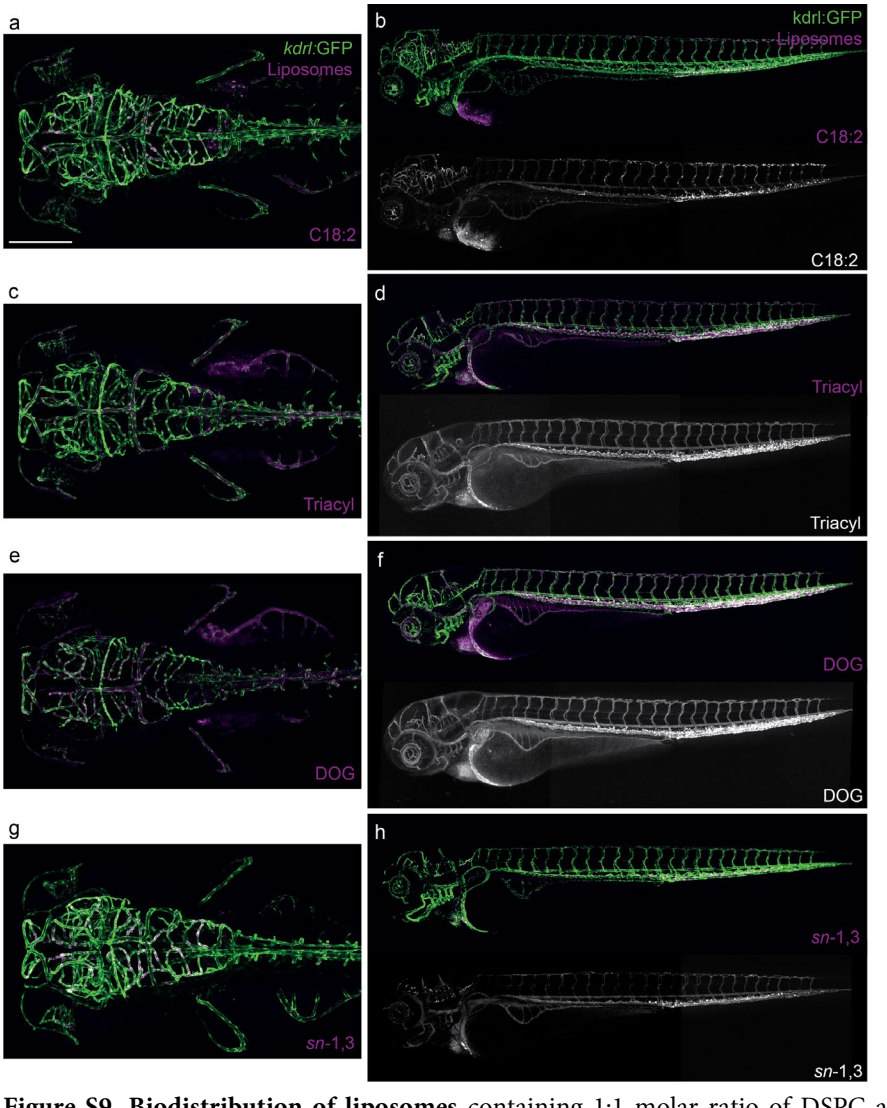

Figure S9. Biodistribution of liposomes containing 1:1 molar ratio of DSPC and **a, b)** C18:2, **c, d)** Triacyl, **e, f)** DOG and **g, h)** *sn*-1,3 in Tg(kdrl:GPF) zebrafish embryos,

expressing GFP in all endothelial cells, in dorsal (10x magnification) and lateral view, 1.5 hpi, at 78 dpf. Liposomes in grey/magenta at 5mM total lipid concentration containing 0.2% DOPE-LR for visualization. Vasculature in green. Scale bar for a, c, e, g: 200 µm.

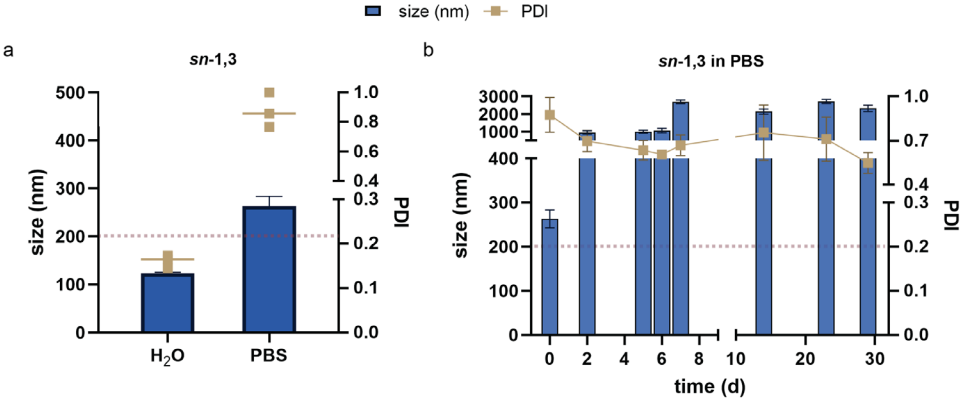

Figure S10. Stability of liposomes containing DSPC and *sn*-1,3 (1:1) made in ddH_2O and PBS. a) Size (nm) and PDI measurement of liposomes containing DSPC and *sn*-1,3 (1:1) made in ddH_2O and PBS. b) Size and PDI of liposomes containing DSPC and *sn*-1,3 (1:1) made in PBS over a period of ~30 days. Red dashed line indicates the threshold of size and PDI relevant for *in vivo* use.

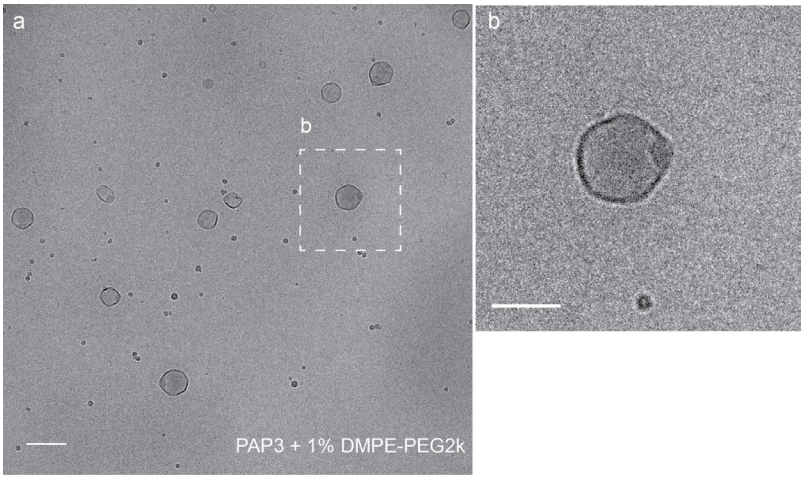

Figure S11. Cryo-TEM images of PAP3 liposomes containing 1% mol DMPE-PEG2k. a) Low magnification image and b) inset from **a** (white box). Scale bars: 200 nm for (a) and 100 nm for (b).

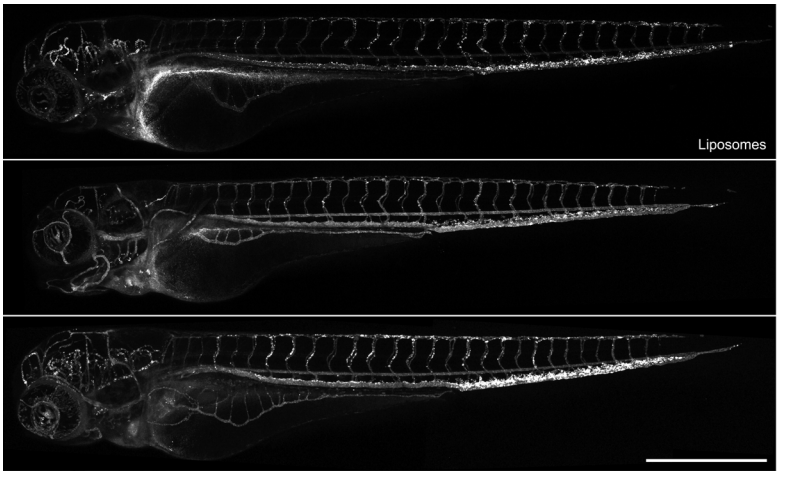

Figure S12. Biodistribution of PAP3 liposomes coated with 1 % mol DMPE-PEG2k in AB/TL zebrafish embryos (wild type), in lateral view, 2.5 hpi at 78 dpf. Liposomes in grey at 5mM total lipid concentration containing 0.2% DOPE-LR for visualization. Scale bar: 500 μm.

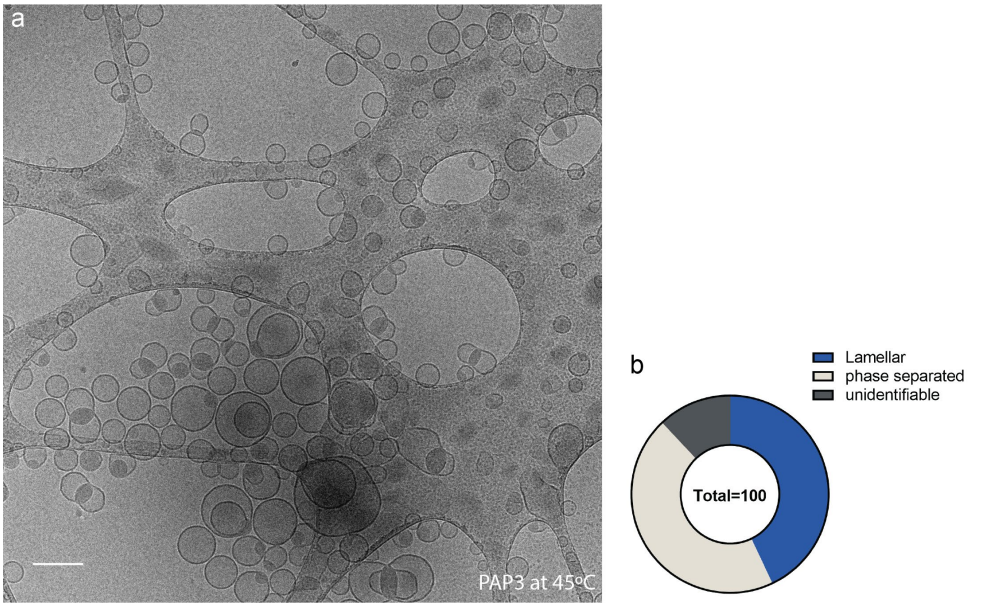

Figure S13. PAP3 liposomes at 45 < T < 65 ºC. a) Cryo-TEM image of PAP3 liposomes cooling to 45 ºC, immediately after formation at 65 ºC. **b)** Quantification of all populations found in the formulation. Quantification based on cryo-TEM image a (N=100). Scale bar = 200 nm.

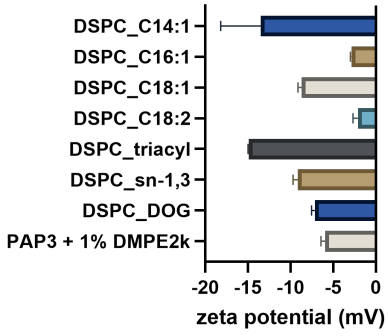

Figure S14. Zeta potential (mV) of stable formulations containing DSPC and DOaG analogues (1:1).

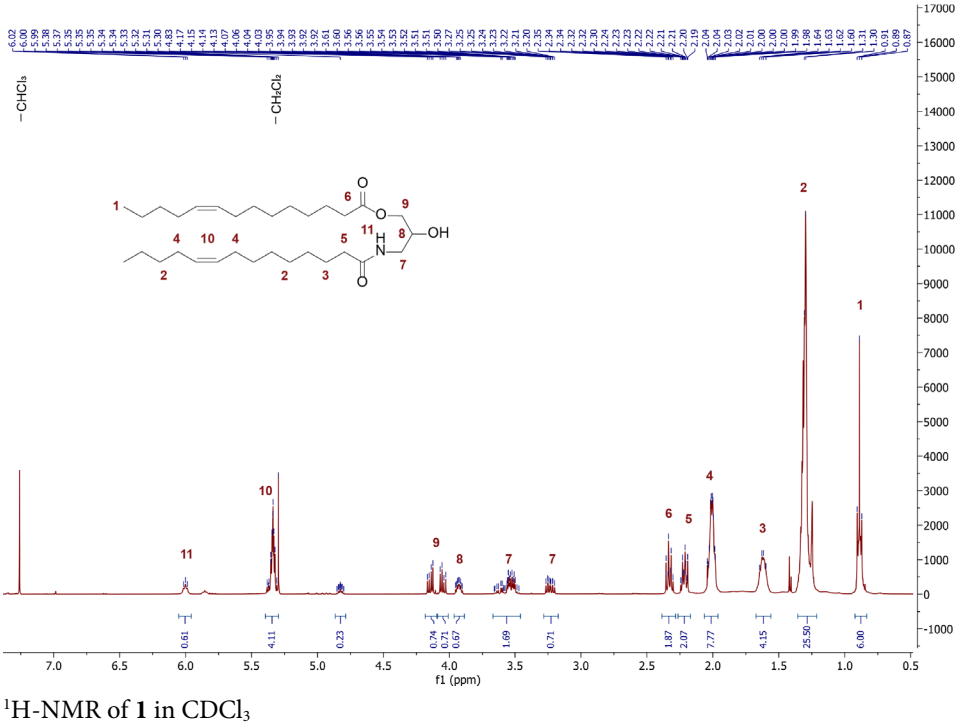

^{1}H-NMR of **1** in $CDCl_3$

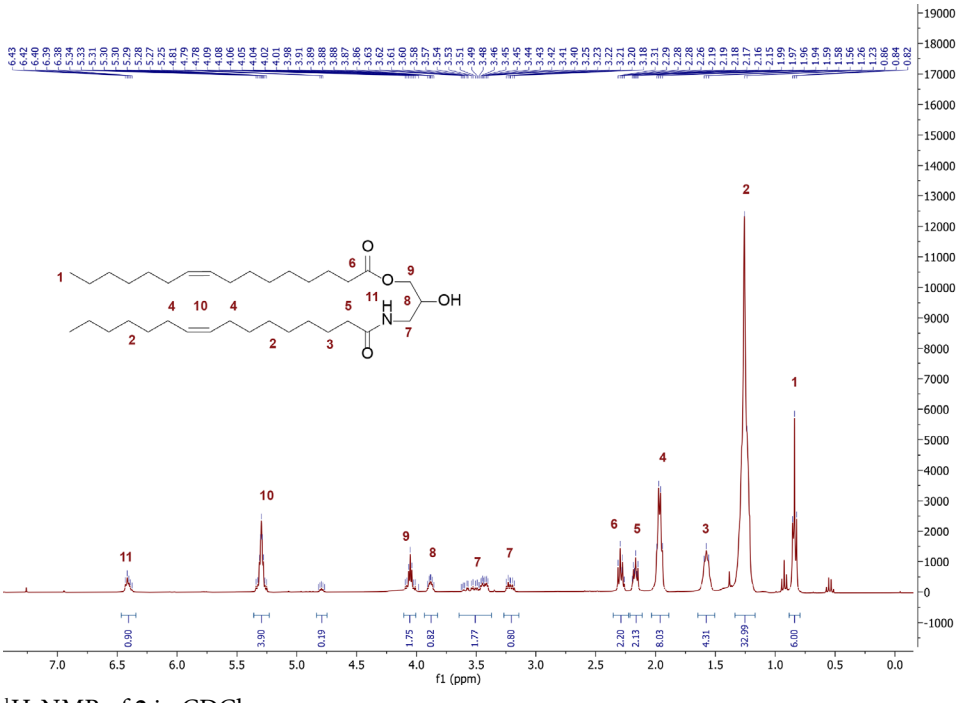

^{1}H-NMR of **2** in $CDCl_3$

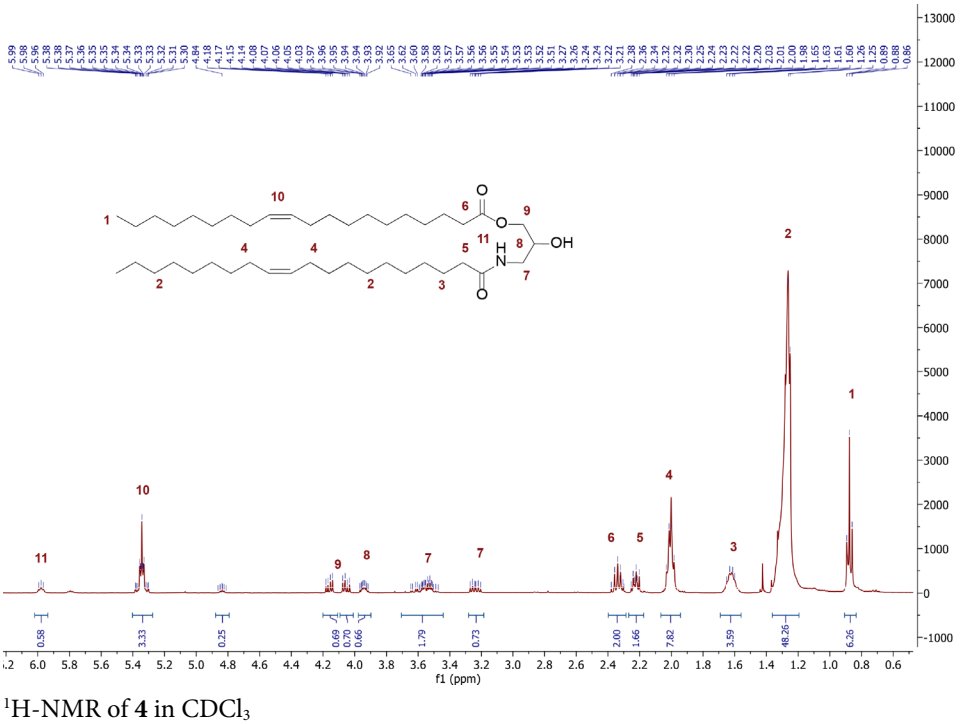

^{1}H-NMR of **4** in $CDCl_3$

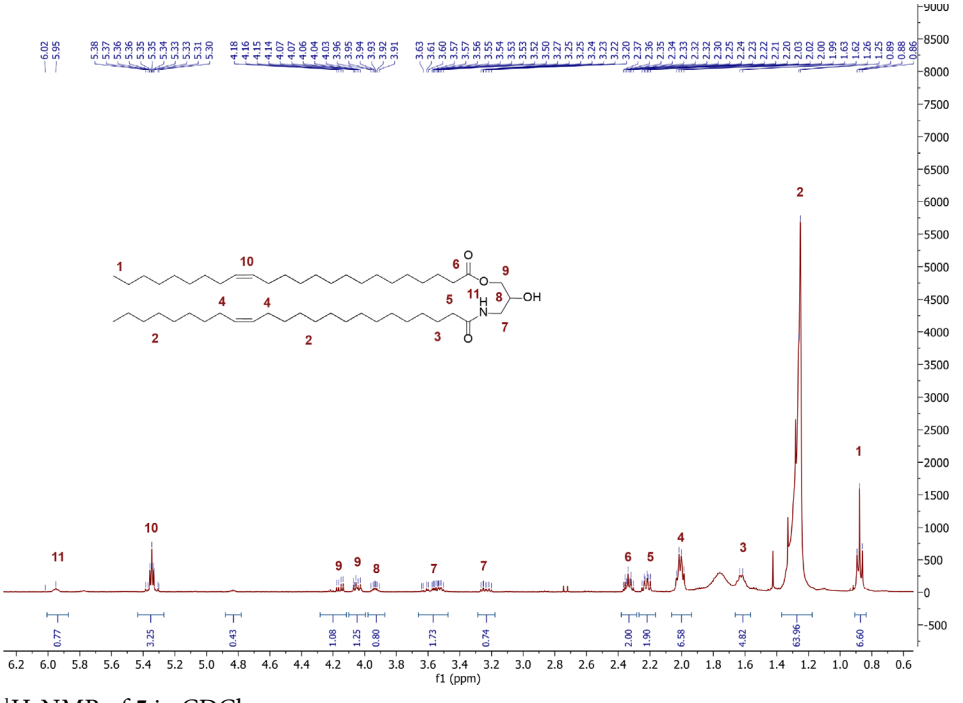

^{1}H-NMR of **5** in $CDCl_3$

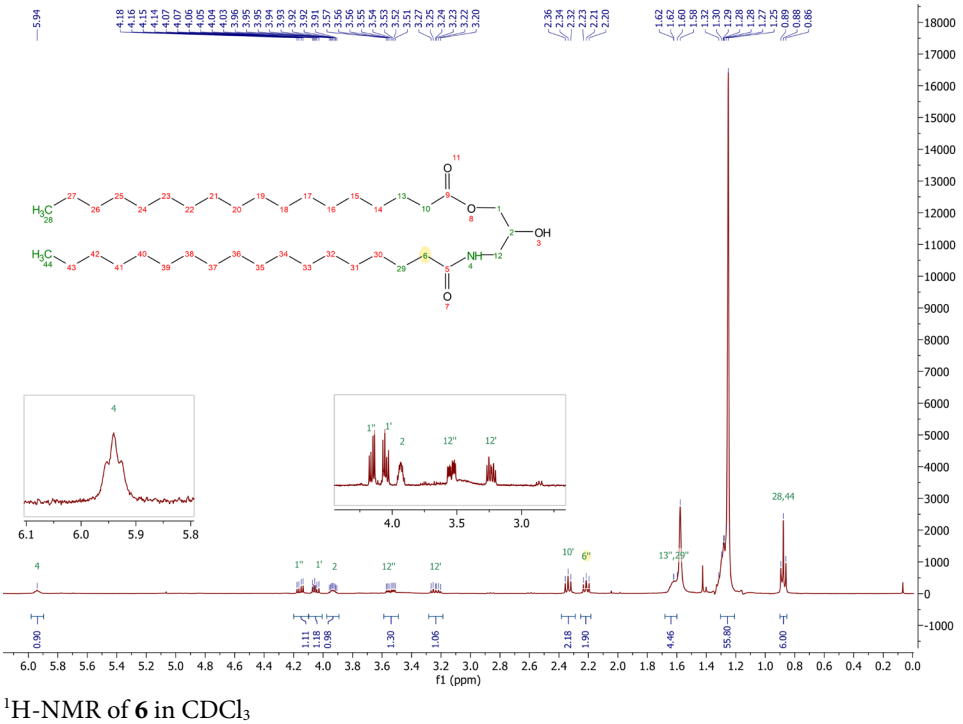

^{1}H-NMR of **6** in $CDCl_3$

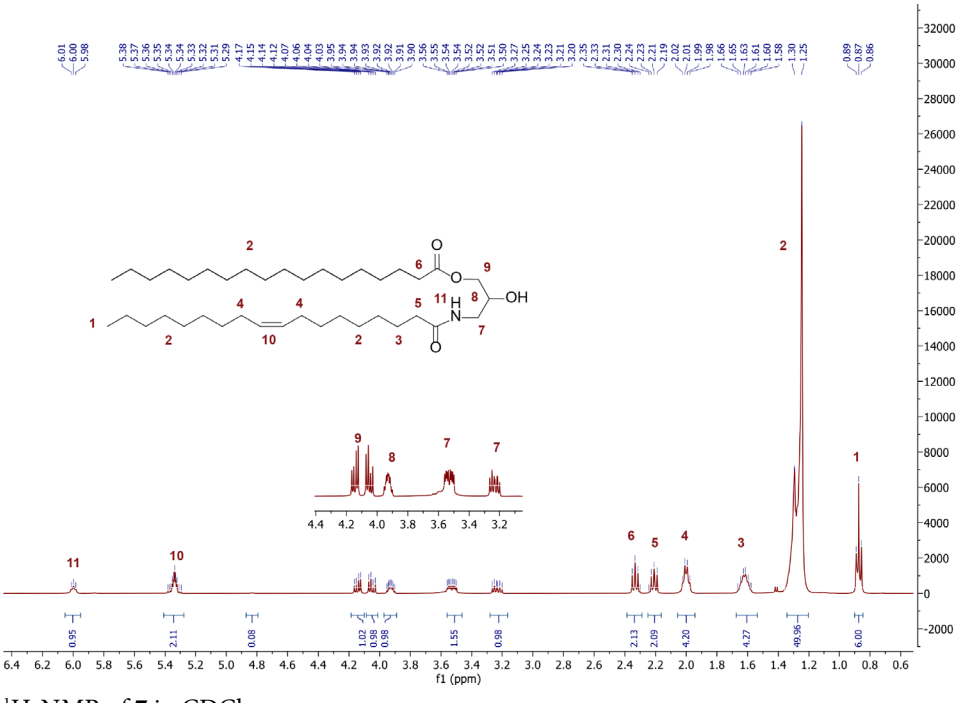

^{1}H-NMR of **7** in $CDCl_3$

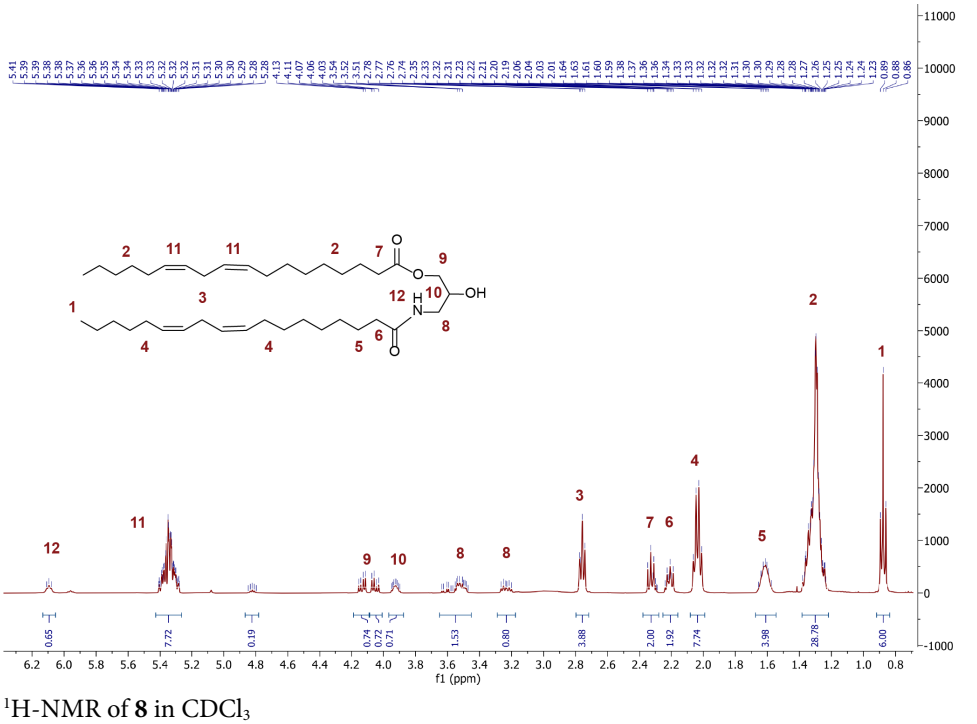

^{1}H-NMR of **8** in $CDCl_3$

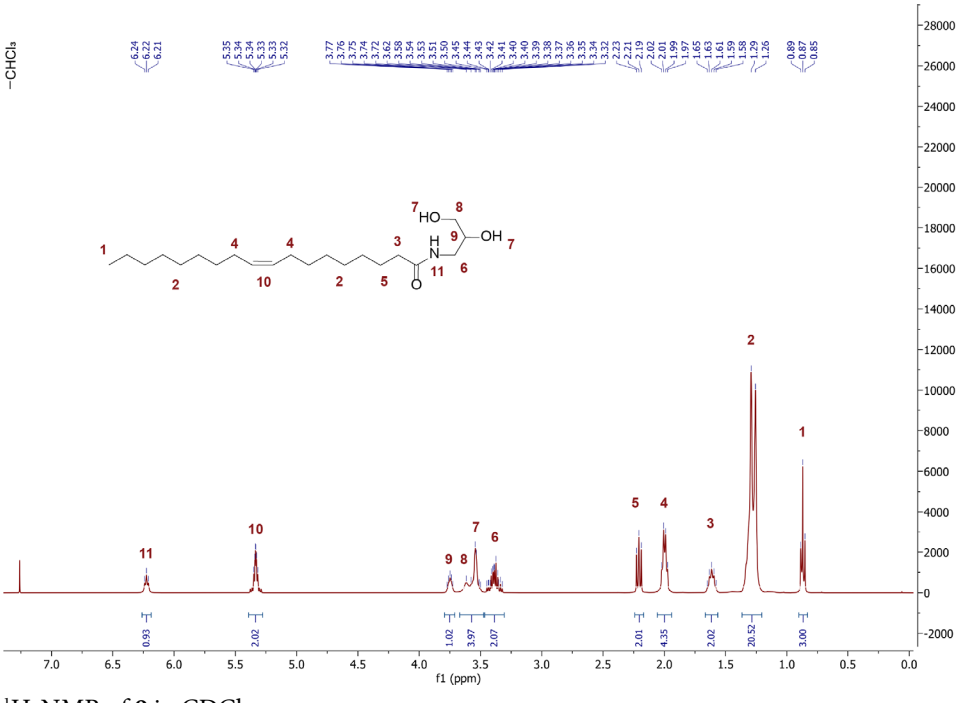

^{1}H-NMR of **9** in $CDCl_3$

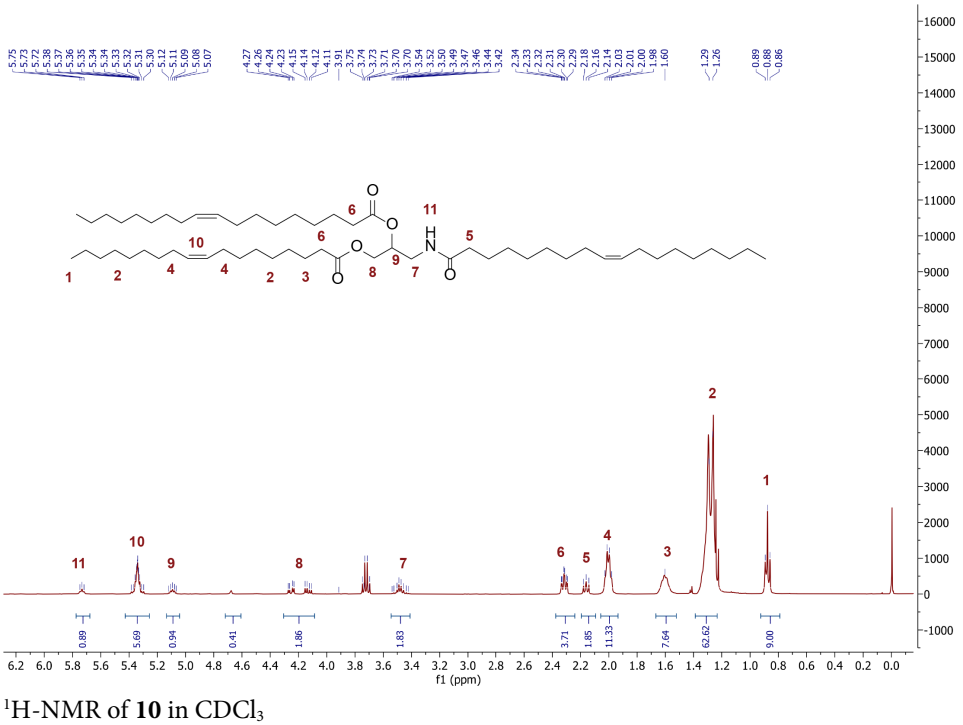

^{1}H-NMR of **10** in $CDCl_3$

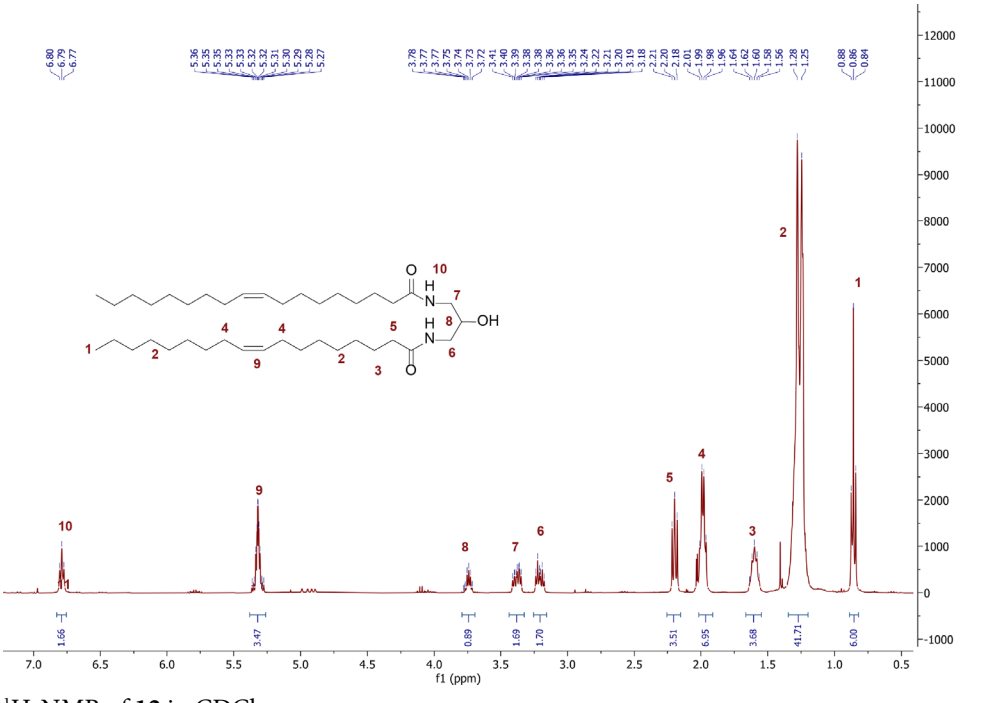

^{1}H-NMR of **12** in $CDCl_3$

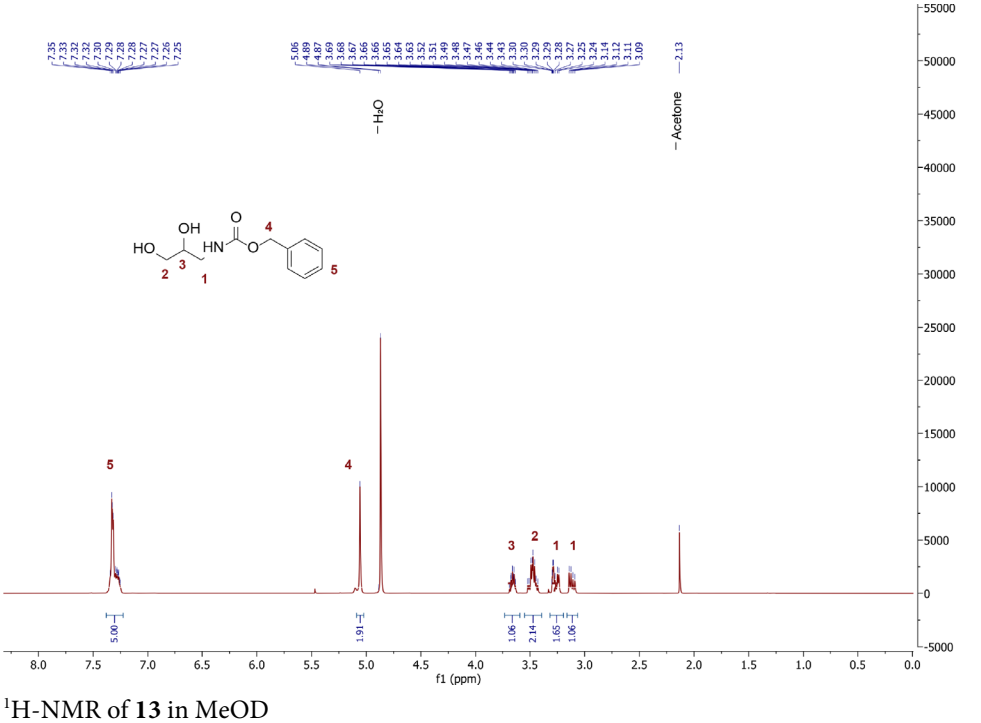

^{1}H-NMR of **13** in MeOD

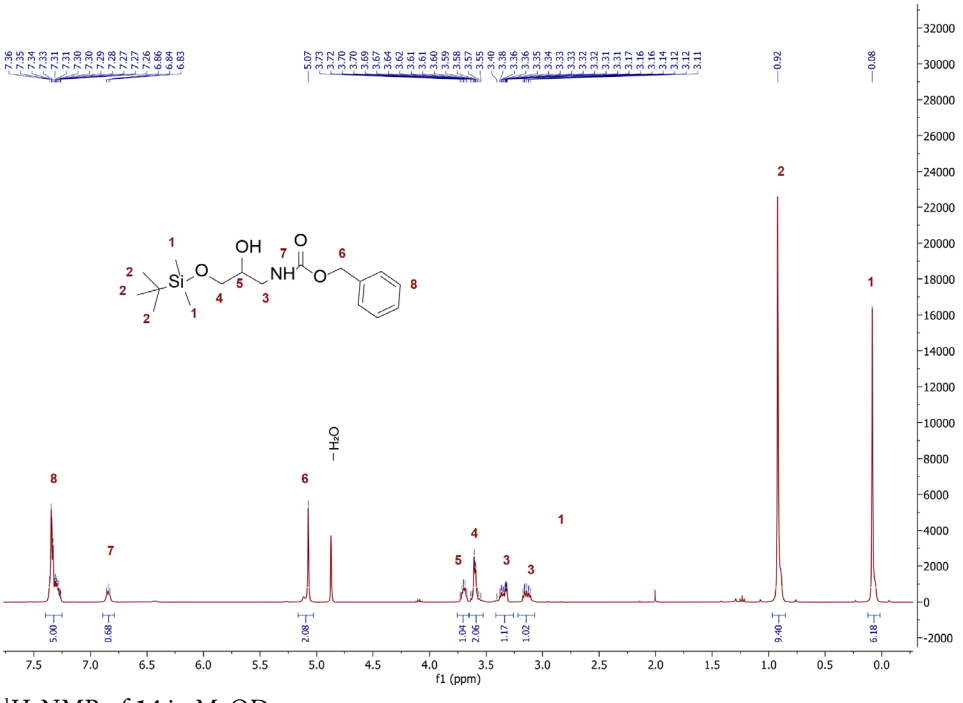

^{1}H-NMR of **14** in MeOD

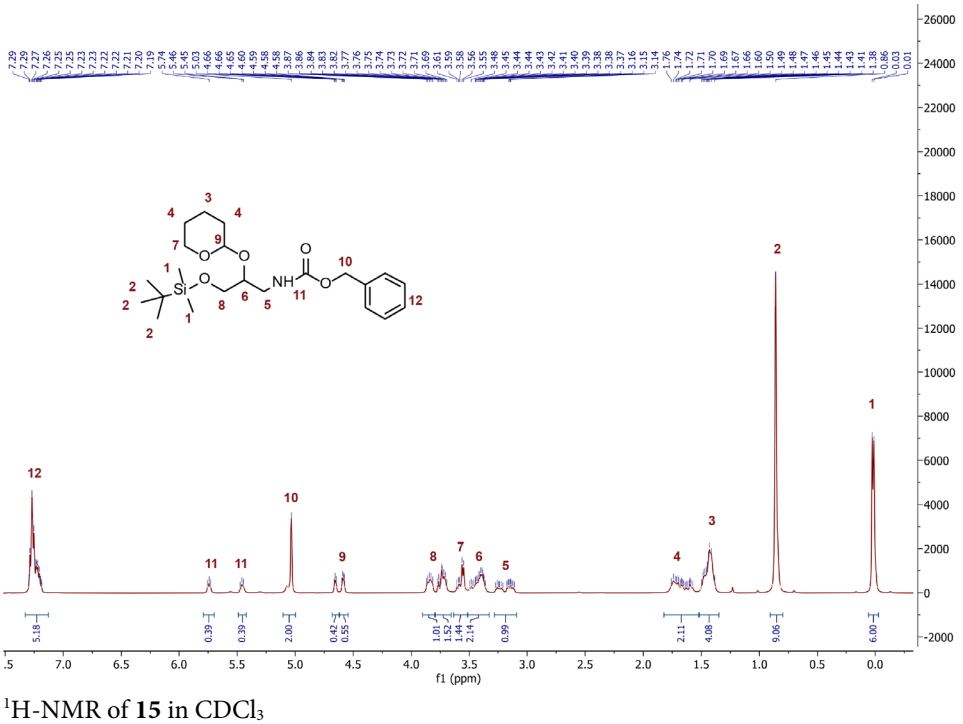

^{1}H-NMR of **15** in $CDCl_3$

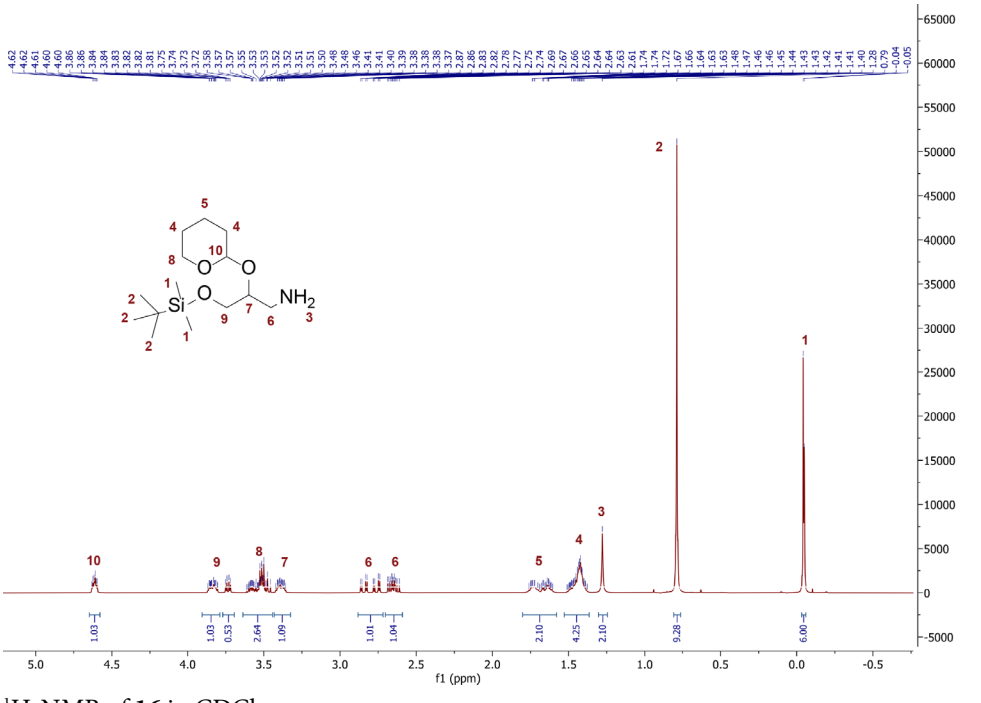

^{1}H-NMR of **16** in $CDCl_3$

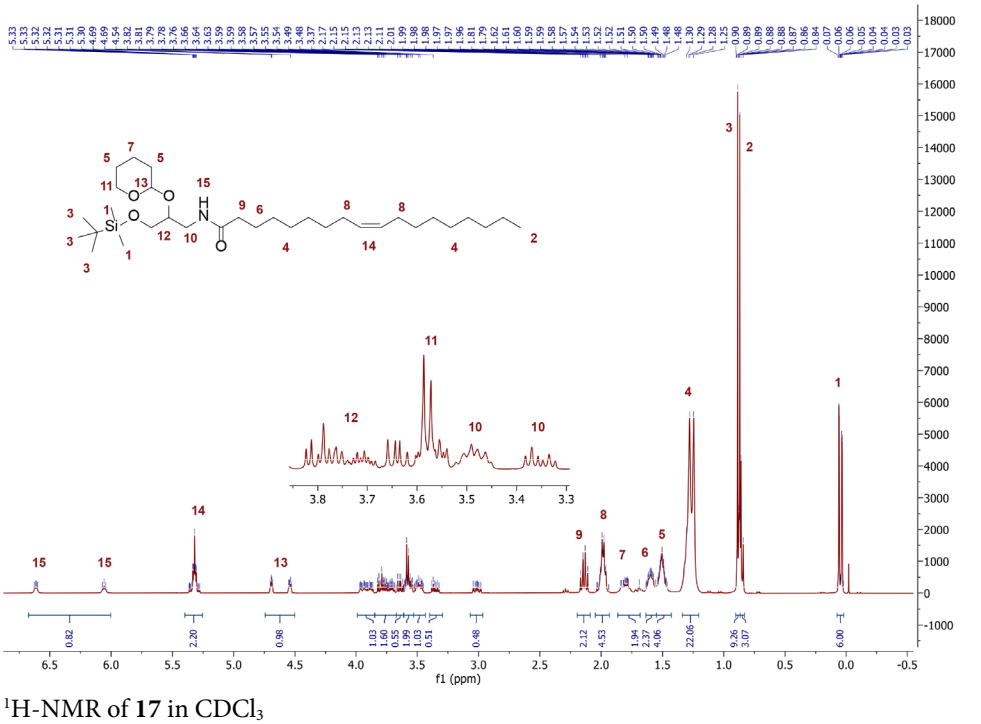

^{1}H-NMR of **17** in $CDCl_3$

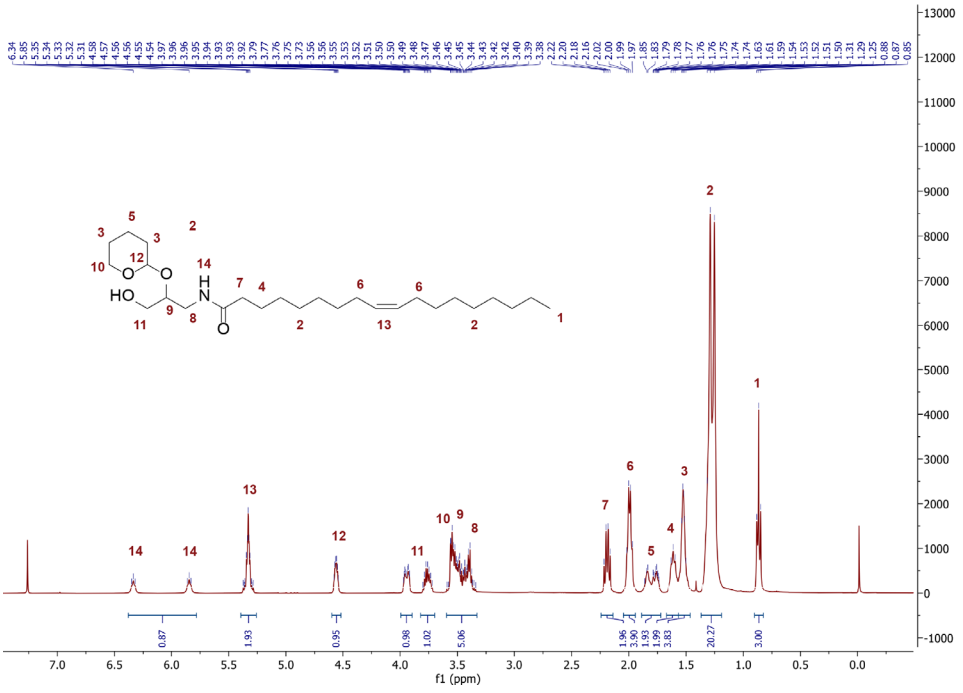

^{1}H-NMR of **18** in $CDCl_3$

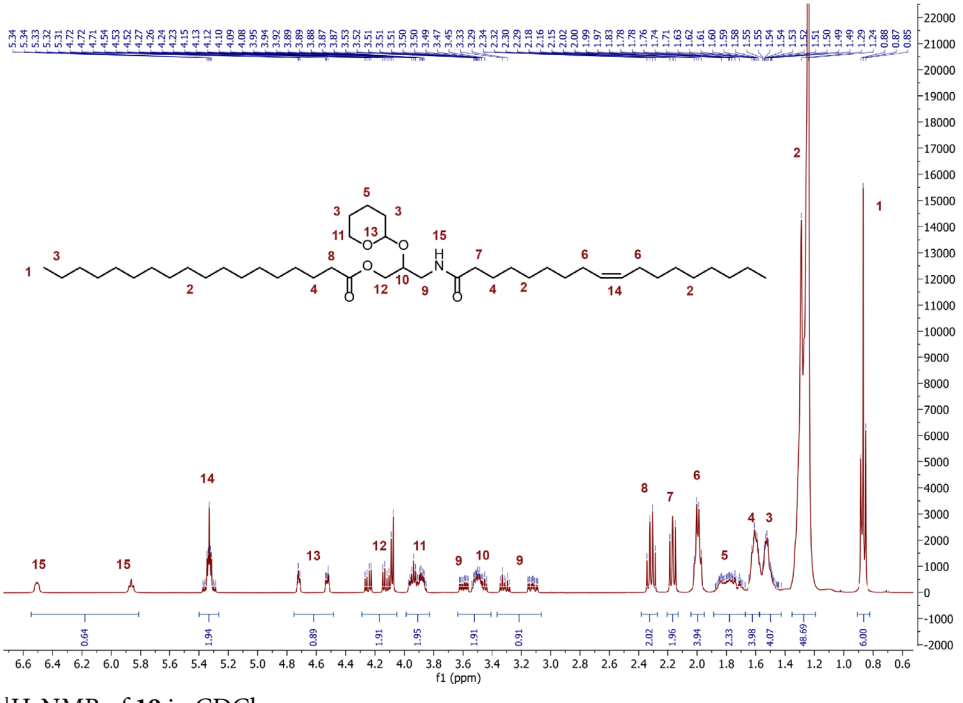

^{1}H-NMR of **19** in $CDCl_3$

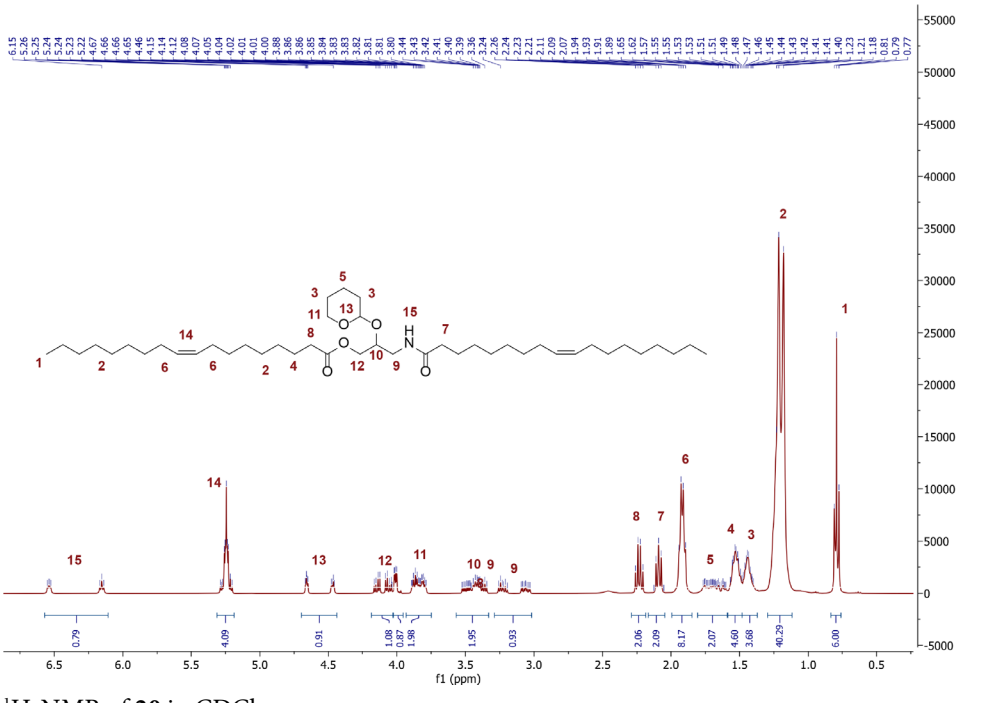

^{1}H-NMR of **20** in $CDCl_3$

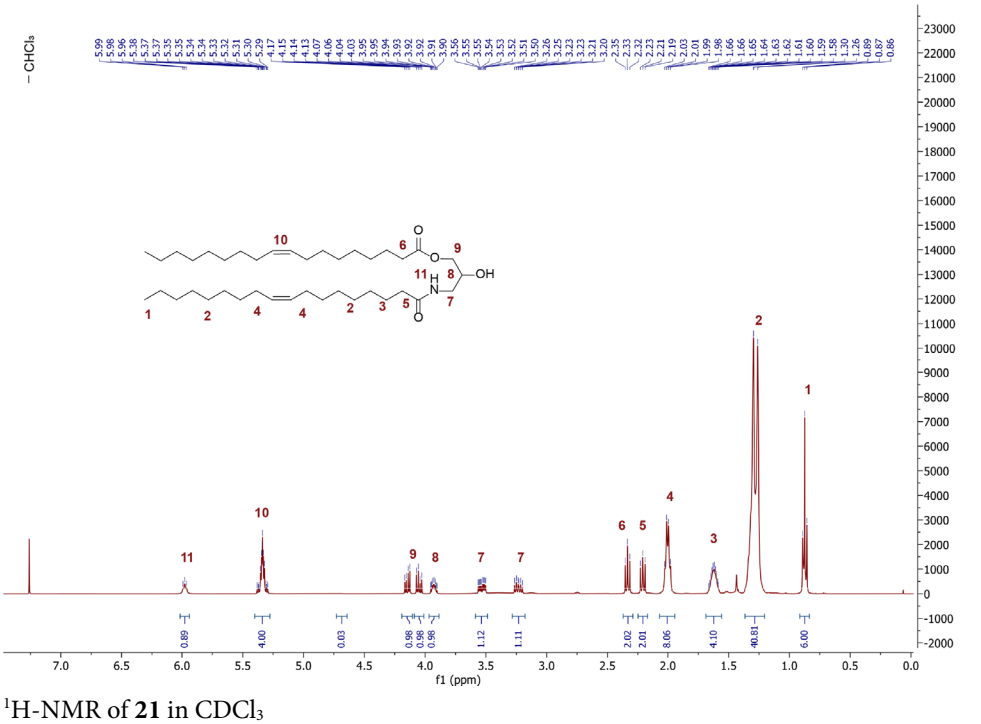

^{1}H-NMR of **21** in $CDCl_3$

4.6 References

1. Duan, X.; Li, Y. Physicochemical Characteristics of Nanoparticles Affect Circulation, Biodistribution, Cellular Internalization, and Trafficking. *Small* **2013**, *9* (9–10), 1521–1532.
2. Mitchell, M. J.; Billingsley, M. M.; Haley, R. M.; Wechsler, M. E.; Peppas, N. A.; Langer, R. Engineering Precision Nanoparticles for Drug Delivery. *Nat Rev Drug Discov* **2020**, *20* (2), 101–124.
3. Blanco, E.; Shen, H.; Ferrari, M. Principles of Nanoparticle Design for Overcoming Biological Barriers to Drug Delivery. *Nat Biotechnol* **2015**, *33* (9), 941–951.
4. Li, M.; Jin, X.; Liu, T.; Fan, F.; Gao, F.; Chai, S.; Yang, L. Nanoparticle Elasticity Affects Systemic Circulation Lifetime by Modulating Adsorption of Apolipoprotein A-I in Corona Formation. *Nat Commun* **2022**, *13* (1), 1–16.
5. Arias-Alpizar, G.; Koch, B.; Hamelmann, N. M.; Neustrup, M. A.; Paulusse, J. M. J.; Jiskoot, W.; Kros, A.; Bussmann, J. Stabilin-1 Is Required for the Endothelial Clearance of Small Anionic Nanoparticles. *Nanomedicine* **2021**, *34*, 102395.
6. Ishiwata, H.; Suzuki, N.; Ando, S.; Kikuchi, H.; Kitagawa, T. Characteristics and Biodistribution of Cationic Liposomes and Their DNA Complexes. *J Control Release* **2000**, *69* (1), 139–148.
7. Cho, E. C.; Xie, J.; Wurm, P. A.; Xia, Y. Understanding the Role of Surface Charges in Cellular Adsorption versus Internalization by Selectively Removing Gold Nanoparticles on the Cell Surface with a I 2/KI Etchant. *Nano Lett* **2009**, *9* (3), 1080–1084.
8. Pattipeiluhu, R.; Arias-Alpizar, G.; Basha, G.; Chan, K. Y. T.; Bussmann, J.; Sharp, T. H.; Moradi, M.-A.; Sommerdijk, N.; Harris, E. N.; Cullis, P. R.; Kros, A.; Witzigmann, D.; Campbell, F. Anionic Lipid Nanoparticles Preferentially Deliver mRNA to the Hepatic Reticuloendothelial System. *Adv Mater* **2022**, *34* (16), e2201095.
9. Campbell, F.; Bos, F. L.; Sieber, S.; Arias-Alpizar, G.; Koch, B. E.; Huwyler, J.; Kros, A.; Bussmann, J. Directing Nanoparticle Biodistribution through Evasion and Exploitation of Stab2-Dependent Nanoparticle Uptake. *ACS Nano* **2018**, *12* (3), 2138–2150.
10. Arias-Alpizar, G.; Kong, L.; Vlieg, R. C.; Rabe, A.; Papadopoulou, P.; Meijer, M. S.; Bonnet, S.; Vogel, S.; van Noort, J.; Kros, A.; Campbell, F. Light-Triggered Switching of Liposome Surface Charge Directs Delivery of Membrane Impermeable Payloads in vivo. *Nat Commun* **2020**, *11*, 3638.

11. Cullis, P. R.; Hope, M. J.; Tilcock, C. P. S. Lipid Polymorphism and the Roles of Lipids in Membranes. *Chem Phys Lipids* **1986**, *40* (2–4), 127–144.
12. Frolov, V. A.; Shnyrova, A. v.; Zimmerberg, J. Lipid Polymorphisms and Membrane Shape. *Cold Spring Harb Perspect Biol* **2011**, *3* (11), a004747.
13. Arias-Alpizar, G.; Papadopoulou, P.; Rios, X.; Pulagam, K. R.; Moradi, M. A.; Pattipeiluhu, R.; Bussmann, J.; Sommerdijk, N.; Llop, J.; Kros, A.; Campbell, F. Phase-Separated Liposomes Hijack Endogenous Lipoprotein Transport and Metabolism Pathways to Target Subsets of Endothelial Cells in vivo. *Adv Healthc Mater* **2023**, *12* (10), e2202709.
14. Papadopoulou, P.; Van Der Pol, R.; Van Hilten, N.; Moradi, M.-A.; Ferraz, M. J.; Aerts, J. M. F. G.; Sommerdijk, N.; Risselada, H. J.; Sevink, G. J. A.; Kros, A. Lipase-Mediated Selective Hydrolysis of Lipid Droplets in Phase-Separated Liposomes. *ChemRxiv* **2023**, DOI : 10.26434/chemrxiv-2023-9q9wh-v3.
15. Semple, S. C.; Akinc, A.; Chen, J.; Sandhu, A. P.; Mui, B. L.; Cho, C. K.; Sah, D. W. Y.; Stebbing, D.; Crosley, E. J.; Yaworski, E.; Hafez, I. M.; Dorkin, J. R.; Qin, J.; Lam, K.; Rajeev, K. G.; Wong, K. F.; Jeffs, L. B.; Nechev, L.; Eisenhardt, M. L.; Jayaraman, M.; Kazem, M.; Maier, M. A.; Srinivasulu, M.; Weinstein, M. J.; Chen, Q.; Alvarez, R.; Barros, S. A.; De, S.; Klimuk, S. K.; Borland, T.; Kosovrasti, V.; Cantley, W. L.; Tam, Y. K.; Manoharan, M.; Ciufolini, M. A.; Tracy, M. A.; De Fougerolles, A.; MacLachlan, I.; Cullis, P. R.; Madden, T. D.; Hope, M. J. Rational Design of Cationic Lipids for siRNA Delivery. *Nat Biotechnol* **2010**, *28* (2), 172–176.
16. Patel, S.; Ashwanikumar, N.; Robinson, E.; Xia, Y.; Mihai, C.; Griffith, J. P.; Hou, S.; Esposito, A. A.; Ketova, T.; Welsher, K.; Joyal, J. L.; Almarsson, Ö.; Sahay, G. Naturally-Occurring Cholesterol Analogues in Lipid Nanoparticles Induce Polymorphic Shape and Enhance Intracellular Delivery of mRNA. *Nat Commun* **2020**, *11* (1), 1–13.
17. Janmey, P. A.; Kinnunen, P. K. J. Biophysical Properties of Lipids and Dynamic Membranes. *Trends Cell Biol* **2006**, *16* (10), 538–546.
18. Siegel, D. P.; Epand, R. M. The Mechanism of Lamellar-to-Inverted Hexagonal Phase Transitions in Phosphatidylethanolamine: Implications for Membrane Fusion Mechanisms. *Biophys J* **1997**, *73* (6), 3089–3111.
19. Cullis, P. R.; Hope, M. J. Lipid Nanoparticle Systems for Enabling Gene Therapies. *Mol Ther* **2017**, *25* (7), 1467–1475.
20. Hafez, I. M.; Cullis, P. R. Roles of Lipid Polymorphism in Intracellular Delivery. *Adv Drug Deliv Rev* **2001**, *47* (2–3), 139–148.

21. Huang, Y.; Gui, S. Factors Affecting the Structure of Lyotropic Liquid Crystals and the Correlation between Structure and Drug Diffusion. *RSC Adv* **2018**, *8*, 6978–6987.
22. Johnsson, M.; Lam, Y.; Barauskas, J.; Tiberg, F. Aqueous Phase Behavior and Dispersed Nanoparticles of Diglycerol Monooleate/Glycerol Dioleate Mixtures. *Langmuir* **2005**, *21* (11), 5159–5165.
23. Popescu, G.; Barauskas, J.; Nylander, T.; Tiberg, F. Liquid Crystalline Phases and Their Dispersions in Aqueous Mixtures of Glycerol Monooleate and Glyceryl Monooleyl Ether. *Langmuir* **2007**, *23* (2), 496–503.
24. Johnsson, M.; Barauskas, J.; Tiberg, F. Cubic Phases and Cubic Phase Dispersions in a Phospholipid-Based System. *J. Am. Chem. Soc.* **2005**, *127* (4), 1076–1077.
25. Goñi, F. M.; Alonso, A. Structure and Functional Properties of Diacylglycerols in Membranes. *Prog Lipid Res* **1999**, *38* (1), 1–48.
26. Campomanes, P.; Zoni, V.; Vanni, S. Local Accumulation of Diacylglycerol Alters Membrane Properties Nonlinearly Due to Its Transbilayer Activity. *Commun Chem* **2019**, *2* (1), 1–8.
27. Alwarawrah, M.; Hussain, F.; Huang, J. Alteration of Lipid Membrane Structure and Dynamics by Diacylglycerols with Unsaturated Chains. *Biochim Biophys Acta Biomembr* **2016**, *1858* (2), 253–263.
28. Goldberg, E. M.; Lester, D. S.; Borchardt, D. B.; Zidovetzki, R. Effects of Diacylglycerols on Conformation of Phosphatidylcholine Headgroups in Phosphatidylcholine/Phosphatidylserine Bilayers. *Biophys J* **1995**, *69* (3), 965–973.
29. Alwarawrah, M.; Dai, J.; Huang, J. Modification of Lipid Bilayer Structure by Diacylglycerol: A Comparative Study of Diacylglycerol and Cholesterol. *J Chem Theory Comput* **2012**, *8* (2), 749–758.
30. Bilayers Edward Goldberg, P. M.; Lester, D. S.; Borchardt, D. B.; Zidovetzki, R. Effects of Diacylglycerols and Ca2+ on Structure of Phosphatidylcholine/Phosphatidylserine Bilayers. *Biophys J* **1994**, *66*, 382–393.
31. Dawson, R. M. C.; Hemington, N. L.; Irvine, R. F. Diacylglycerol Potentiates Phospholipase Attack upon Phospholipid Bilayers: Possible Connection with Cell Stimulation. *Biochem Biophys Res Commun* **1983**, *117* (1), 196–201.
32. Holme, M. N.; Rashid, M. H.; Thomas, M. R.; Barriga, H. M. G.; Herpoldt, K. L.; Heenan, R. K.; Dreiss, C. A.; Bañuelos, J. L.; Xie, H. N.; Yarovsky, I.; Stevens, M. M. Fate of Liposomes in the Presence of Phospholipase C and D: From Atomic to Supramolecular Lipid Arrangement. *ACS Cent Sci* **2018**, *4* (8), 1023–1030.

33. Strijkers, G. J.; Mulder, W. J. M.; van Heeswijk, R. B.; Frederik, P. M.; Bomans, P.; Magusin, P. C. M. M.; Nicolay, K.; Nicolay, · K; Nmr, B.; Bomans, · P. Relaxivity of Liposomal Paramagnetic MRI Contrast Agents. *MAGMA* **2005**, *18*, 186–192.
34. Gómez-Fernández, J. C.; Corbalán-García, S. Diacylglycerols, Multivalent Membrane Modulators. *Chem Phys Lipids* **2007**, *148*, 1–25.
35. Da Silva Sanchez, A. J.; Zhao, K.; Huayamares, S. G.; Hatit, M. Z. C.; Lokugamage, M. P.; Loughrey, D.; Dobrowolski, C.; Wang, S.; Kim, H.; Paunovska, K.; Kuzminich, Y.; Dahlman, J. E. Substituting Racemic Ionizable Lipids with Stereopure Ionizable Lipids Can Increase mRNA Delivery. *J Control Release* **2023**, *353*, 270–277.
36. Hatit, M. Z. C.; Dobrowolski, C. N.; Lokugamage, M. P.; Loughrey, D.; Ni, H.; Zurla, C.; Da Silva Sanchez, A. J.; Radmand, A.; Huayamares, S. G.; Zenhausern, R.; Paunovska, K.; Peck, H. E.; Kim, J.; Sato, M.; Feldman, J. I.; Rivera, M. A.; Cristian, A.; Kim, Y. T.; Santangelo, P. J.; Dahlman, J. E. Nanoparticle Stereochemistry-Dependent Endocytic Processing Improves in vivo mRNA Delivery. *Nat Chem* **2023**, *15*, 508–515.
37. Jin, S. W.; Beis, D.; Mitchell, T.; Chen, J. N.; Stainier, D. Y. R. Cellular and Molecular Analyses of Vascular Tube and Lumen Formation in Zebrafish. *Development* **2005**, *132* (23), 5199–5209.
38. Arias-Alpizar, G.; Bussmann, J.; Campbell, F. Zebrafish Embryos as a Predictive Animal Model to Study Nanoparticle Behavior in vivo. *Bio Protoc* **2021**, *11* (19), e4173.